Investigation of Qubit Isolation in a Rare-Earth Quantum Computer

Annabel Alexander

A thesis submitted in part fulfilment of
the requirements for the degree of
Bachelor of Science with Honours, from
the Department of Physics,
The Australian National University

November, 2002

Declaration

This thesis is an account of research undertaken at The Research School of Physical Sciences and Engineering, The Australian National University, Canberra, Australia.

Except where acknowledged in the customary manner, the material presented in this thesis is, to the best of my knowledge, original and has not been submitted in whole or part for a degree in any university.

Annabel L. V. Alexander
November , 2002

Acknowledgements

I would like to give a huge thanks to both my supervisors, Prof. Neil Manson and Dr Matt Sellars, for always being there with new approaches and ideas when things started to go bad. Also for their help and guidance throughout my stay at the LPC and for both reading the countless copies of my thesis I kept handing them. I would also like to thank them both for introducing me to the wonderful world of rare-earth quantum computers.

I would like to thank all those people who ever fed me during this year, Alex and Reanna for the weeks in the lab when dinner was always there. Ira for all the jaffles when I was really desperate and there was no food to be had.

Thanks all those people who ever came depressive drinking with me.

A big thank you to all the PhD students in the Laser Physics Centre. Particularly Elliot for his hedgehog, even though we killed it, Jevon for always answering my endless theoretical, unix and matlab related questions and for Darryl for always being ready when a beer was required.

Thank you to all those people who read through my thesis and offered suggestions; Elliot, Ira, Jevon, Darryl and Tristram (even though you were in Italy at the time).

Ian McRae and John Bottega for their skills at repairing and the endless supply of helium.

I'd like to thank all my fellow honours students who made this year so enjoyable, especially for an honours year.

Finally I would like to thank all my friends and family who were so understanding and supportive throughout the year and for putting up with all my stress.

Abstract

The general aim of this project was to contribute to the work being done at the Laser Physics Centre in the Research School of Physical Sciences and Engineering in their quest to build a quantum computer. Perturbations on the decoherence time were studied with a number of different methods. These experimental methods were also theoretically modeled. It was found that in no cases was there a clear change above the uncertainties set by experimental errors, however upper bounds were able to be determined. Optical perturbation of the crystal was found to have an upper interaction strength of 40Hz, while the upper bound on the electric dipole-dipole interaction is 2Hz.

Raman echoes were achieved for the first time in this lab and have the longest reported coherence time due to an applied magnetic field.

Contents

Introduction

1.1 Motivation

Classical computers have been improving at a fantastic rate, with speed increasing every year and components becoming smaller and smaller. This improvement may eventually reach a limit in which case an entirely new direction will need to be taken with respect to computing power, quantum computers. In a classical computer data is represented with a binary code of zeroes and ones, known as bits. In this case there are two states that are mutually exclusive and this idea is also present in the quantum world. The difference between a classical and quantum computer is due to the superposition principle. In a quantum computer it is also possible to have a superposition of the two states. The spin orientation of a system, the polarisation of a photon or the outcome of a photon at a beam-splitter are all examples of quantum states that can exist as a superposition. Instead of using bits to represent the data, in a quantum computer we have quantum bits, or qubits for short, which are the quantum states of a 2-level system. In the system investigated at the Laser Physics Centre these states are the nuclear spin states, 'up' or 'down', and are written as $|1\rangle$ or $|0\rangle$, respectively.

At the moment the fastest classical computers employ parallelism to increase their speed. Parallelism is when multiple processors are performing the same calculation on different inputs. Quantum computers are inherently parallel machines, due to the superposition principle. A quantum computer with n qubits is able to perform, in one computational step, an operation on 2^n different input numbers, returning a superposition state of all the outputs. The same sized classical computer would need to perform the operation 2^n times on the different inputs, or have 2^n processors.

In order to achieve a working quantum computer there are five properties the system needs to satisfy, [1]:

1. the superposition states of the qubits must be long-lived quantum states
2. these states must be able to be externally manipulated in order to perform calculations
3. it must be possible to initialise the state
4. the system can be read-out
5. the interactions between the qubits must be controllable

For the superposition states to be long-lived there should be minimal interactions between the system and the environment. When the system interacts with the environment

the superposition of the qubits evolves to a mixture of states. This process is known as dephasing and the time taken for the qubits to dephase is known as the coherence time. Maximising the coherence time will increase the time during which coherent operations may be performed before the stored information is lost due to dephasing. The practical difficulty with building a quantum computer is that the system needs to be isolated from the environment to reduce decoherence and yet not be so isolated that information can't be stored or manipulated. While uncontrolled interactions with the environment lead to decoherence there must be controlled interactions to perform operations. My project focused on the perturbation to information stored in one qubit from uncontrolled interactions when operating on other qubits. These perturbations will result in errors in the computer's operations. The aim was to develop and demonstrate techniques to measure these uncontrolled interactions and to estimate their magnitude.

1.2 Solid State Systems

The system that was chosen to study was a solid state system, where the basic units are the nuclear spins. The nuclear spin levels don't interact much with the surrounding environment. Simplistically this is because the wavefunction of the nuclear states is small and there is little overlap with the "environment". The result is that decoherence is kept to a minimum. Decoherence is caused by the uncontrolled interaction of the system with the surrounding environment so in a solid-state system that surrounding environment is the lattice. The main causes of dephasing are changing magnetic fields at the centre, due to its nuclear and electronic spins. This means that only other ions with spins in the lattice will affect the dephasing.

Choosing a solid state system means it is scalable as additional qubits are easy to add to the lattice. There has been more interest of late paid to solid-state systems for a quantum computer and there are two main approaches; the rare-earth system,[2] and the silicon based system [3], [4]. We chose to study the rare earth system with the major difference from the silicon based approach being it is an optically active centre. There are optical transitions from the different ground state nuclear spin levels that share a common electronic level. The electronic (or optical) level is used to manipulate and read-out the

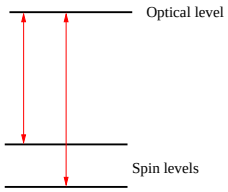

Figure 1.1: The spin states share a common electronic level

spin state.

This electronic level is important since the nuclear levels of the different qubits interact only weakly and so this electronic level is necessary for the qubit manipulation. Due to the low symmetry of our system the nuclear spin states are mixed. The nuclear spin labels are then no longer good quantum numbers and hence there are different labels in the ground and excited electronic states. So one can obtain transitions between different nominal nuclear spin states. This allows the information to be accessed optically and hence can be obtained with optical methods rather than NMR ones. Due to the higher energies of

optical photons over rf photons the quantum efficiency of detection using optical methods is much higher than can be achieved using standard NMR techniques.

The difficulty with using nuclear spins for quantum computing is the very property that makes them so attractive, their isolation from their surrounds. Although good isolation from the environment is required it is also necessary for the qubits to interact with each other to perform gate operations. The interaction between the nuclear spin states of the centres is typically only kHz or less depending on their separation. The common optical level can be used to avoid the problem of the weak interactions between the spin qubits as it can be used to transfer coherence from the spin states to the electronic states. Each centre can be thought of as two qubits; a spin qubit and an electronic qubit. Although the spin-spin interaction between two centres is weak, there is a strong electric dipole-dipole interaction associated with the electronic states. The idea is to use the spin qubits for

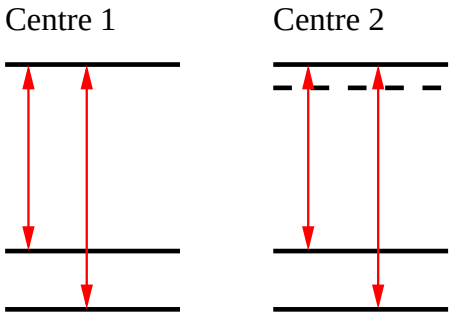

Figure 1.2: Optical excitation of Centre 1 causes a shift in the optical transition in Centre 2

storage and the electronic qubit for 2-qubit gate operations. This procedure is an essential component of the rare earth quantum computer as originally proposed by Sellars [5] and developed by Kroll et al. [6]. The question that this thesis asks is what happens to a third qubit which is in the vicinity of centres being optically manipulated. This work is investigating the dominant interactions involved and estimating their strengths.

1.3 Rare-Earth Doped System

The system that was eventually used in this project was praseodymium in a yttrium orthosilicate lattice, $Pr^{3+} : Y_2SiO_5$. Praseodymium is the optically active ion and is taken from the Lanthanide series. This system is similar to an ion-trap since the electronic transitions are insulated from the lattice [7]. By cooling the crystal the energy of the phonons in the lattice is too low to be able to flip the spins. Hence many body interactions between phonons and the ions are necessary and these are improbable interactions. For the purposes of this investigation this crystal can be thought of as a yttrium lattice with a substitutional praseodymium ion as in figure 1.3.

The crystal is drawn as such, without the silicon, natural abundance is 95%, and oxygen ions, natural abundance is 99%, because these ions are both even-even nuclei and hence have no nuclear or electronic spin. This lack of spin means these ions constitute only a static environment for the Pr^{3+} ions. It is only other spins which are important for interactions in the crystal. Since the Pr^{3+} ions have a nuclear spin of 5/2 they have a magnetic moment and it is this moment which makes the ion sensitive to other spins.

In this quantum computing situation the coherent information is stored in the superposition of the nuclear spin states of the Pr^{3+} ion which have been shown to have a

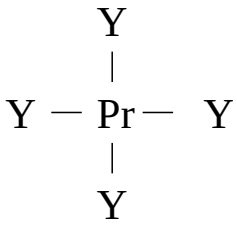

Figure 1.3: Pr lattice structure

decoherence time as long as 82ms [8], satisfying criteria 1. This system has three hyperfine levels in both the ground and excited states as in figure 1.4. The two-fold degeneracy of

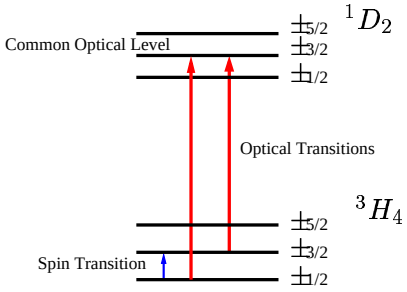

Figure 1.4: Pr level scheme

these levels is lifted in the presence of a magnetic field. Though there are six states in the excited electronic level, in the presence of a magnetic field, we are concerned with only one of these six states. Due to mixing, resulting from the low symmetry of the crystal field there are optical transitions between electronic states of different spin states, see figure 1.4. It is this common electronic level which is used for optical manipulation and read-out of the spin states, as required by criteria two and four. Initialisation of the system is performed through optical pumping, to ensure all the ions are in the ground state, meeting criteria three. In the previous section we have seen how controlled interactions are possible, satisfying criteria five. The focus of this project was to investigate how criteria one, the coherence time of the states, was affected by performing any of the items two-five.

The study could be made for various rare earth ions as several have the same hyperfine features and can be at low symmetry sites. However Pr^{3+} was chosen for the centre as it has a number of advantages over the other rare-earth ions. Pr^{3+} has a relatively strong optical transition with a coherence time of 111μs, which is close to the lifetime limit of 328μs ($2 \times T_1$) [9], where T_1 is the lifetime of the state. This relatively strong transition strength means that, with readily available laser power, it is possible to create large coherences between the levels using light pulses much shorter than the coherence time. This means that one can create coherence in the spin levels without introducing extra dephasing from the optical levels, which should keep dephasing to a minimum. Rabi periods of less than 0.1μs can be achieved using a cw, frequency stabilised dye laser. A consequence of the long optical coherence time compared to the Rabi period is that resonant Raman techniques can be used to create coherences in the spin levels.

1.4 Interactions

In this work I was concerned with how one nuclear spin is affected when the spin or electronic state of another centre is changed. The centre can be affected through three interactions:

- magnetic dipole-dipole
- electric dipole-dipole
- electric dipole-quadrupole

1.4.1 Magnetic Dipole-Dipole

The Pr^{3+} ion has a magnetic dipole moment due to its spin and hence there are magnetic dipole-dipole interactions with the surrounding Pr^{3+} nuclei. The enhanced magnetic moment of the nucleus depends on the electronic state, so optical excitation of one ion will change the magnetic interaction with the magnetic dipole moment of the nearby ions. This causes perturbations on the nuclear spin states of the surrounding ions and is estimated in later chapters.

1.4.2 Electric Dipole-Dipole

The Pr^{3+} ion possesses an electric dipole moment with a direction and magnitude dependent on the electronic state of the ion, [10]. Hence optically exciting the ion will change its electric dipole moment. Further it means that the optical transition has a linear Stark shift:

$$\Delta\nu = \vec{E} \cdot \Delta\vec{p} \tag{1.1}$$

where Δp is the change in the dipole moment between the ground and excited electronic states. Eu^{3+}, which is another rare-earth ion proposed for use in quantum computing, has a Δp of $\sim$34kHzV^{-1}m [10]. The Pr^{3+} is thought to have a similar moment, though the value is currently unknown. Since the electric dipole moment depends on the electronic state of the ion then transitions between the electronic levels then possess a linear Stark shift. Hence optically exciting an ion will change the dipolar field surrounding it and shift the optical excitation frequency of any other Pr^{3+} ion in the vicinity. This interaction is dipole-dipole and so it varies according to $\sim 1/r^3$, so Pr^{3+} ions further away will feel the effect less. The 2-qubit gate operations, from section 1.2, exploit this interaction by operating on the stored information via these optical electric dipole-dipole interactions.

The above has described the electronic dipole-dipole interaction that is exploited in order to perform gate operations, but the electric dipole moment will also depend on the nuclear spin state of the ion, to what degree is unknown. It is expected to be very small due to the weak coupling of the nucleus with the electronic wavefunction. This dependency means that optical excitation will cause a linear Stark shift in the nuclear states of surrounding ions. However it needs to be measured or confirmed and is reported on later.

1.4.3 Electric Dipole-Quadrupole

This interaction is due to the fact that the nucleus has an electric quadrupole moment hence the nuclear spin states are sensitive to the electric field gradient. A change to the

electronic state of one ion causes a change to its electric dipole moment. This change then causes a perturbation on the electric field gradient of other ions in the vicinity. Hence the electric quadrupole moment of these nearby ions are affected by optical excitation of this ion. An estimate as to the size of this interaction will be made later.

1.4.4 Pr-Y Interaction

The techniques used to measure the ion-ion interactions rely on observing changes to the decoherence. The resolution of these measurements will be limited by the background decoherence mechanisms. The main background mechanism is the interaction between the Pr^{3+} ions and the Y ions. At the concentrations we work at, of 0.05% Pr^{3+}, the Pr-Y interaction is the dominate dephasing mechanism.

The Y ions have a nuclear spin of 1/2 and so are constantly mutually spin-flipping amongst themselves. This reorientation is due to the energy conserving spin-flips of the Y ions. This creates random time variations in the magnetic field seen by the Pr^{3+} ions, which result in random Zeeman shifts, perturbing the transition frequency of the Pr^{3+}. We would expect there to be mutual spin flips between the Pr^{3+} ions, resulting in dephasing, but since the Pr-Y interaction is the dominant interaction it determines the coherence time. A similar effect is seen in reference [11], though there the effect is with Fluorine rather than Yttrium. On this time scale the Pr^{3+} ions do not undergo any mutual spin flips and so do not contribute to the dephasing in this way, [12].

1.5 Experiments

I have investigated the Pr-Pr interactions in the lattice through excitation with rf fields and light. I measured the effect excitation of one subgroup of ions had on the coherence of another group, a situation which will be encountered when operating a quantum computer.

The different subgroups of nuclear spin states are selected in the frequency domain, not the spatial domain. Due to inhomogeneous broadening of the optical line of the ions they are all slightly detuned from one another. In figure 1.5(b) the red lines correspond to one subgroup of ions and the blue lines with another. By selecting the excitation frequency it is then possible to select different subgroups of ions. In the crystal there are many Pr^{3+} ions randomly spaced as seen in figure 1.5. The blue circles in figure 1.5(a) represent ions

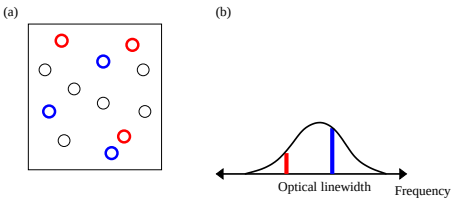

Figure 1.5: (a)The blue circles are on-resonant Pr^{3+} ions while the red are off-resonant ions (b)Blue line is on-resonant frequency of blue ions, red line is off-resonant frequency of red ions

with information stored in their spin states. This set of ions are on resonance with the applied laser beam, while the red subgroup of ions is detuned from this frequency. In a quantum computer information will be stored in the spin states of one set of qubits which could be perturbed by optical operations on a different set. These operations on the other qubits shouldn't interfere with the information stored in the initial set. The aim of this project was to investigate whether this information would be affected by other operations.

This was done by exciting the red subgroup of ions, with rf or light, and measuring how it affects the on-resonance blue subgroup. A similar idea was investigated by Huang et al [13] and Altner et al [14] in the rare-earth system. These groups studied the effect optical excitation of off-resonant ions had on the coherence time of the electronic level of neighbouring ions, while we were studying the effect on the nuclear spin levels. In order to investigate this the main property that was measured was the coherence time of the subgroup. If the other Pr^{3+} ions are affecting the on-resonance group than this interaction will be seen in a change in the coherence time.

There are a number of different methods used to measure the coherence, but I have concentrated on Hahn 2-pulse spin echoes which were first developed in 1950 [15] and are applicable to inhomogeneously broadened systems. The coherence must be set up between the ground and excited hyperfine levels and is achieved by a resonant rf $\pi/2$ pulse. This is followed by an rf π pulse. The $\pi/2$ pulse puts the ions in a superposition of the spin-up and -down states. The ensemble then starts to dephase. When the sample is excited with the π pulse all the spins are flipped through 180° and the dephasing is reversed. After a certain time has elapsed, equal to the time between the $\pi/2$ and the π pulse, the ions are all in phase again and so a signal is emitted, giving the spin echo. By measuring the size of this spin echo for varying time delays it is possible to plot out an exponential decrease where the time constant is the coherence time of the system.

The intention of the experiments was to determine whether the above dephasing time was modified in any way by a perturbing field associated with other operations on the crystal. A modified dephasing will be seen in a faster decay of the echo amplitude. The spin echo is the basis of the techniques being developed in order to study the Pr-Pr interactions.

In 1983 a new method for detecting nuclear spins was developed, the Raman Heterodyne method, [16] which creates the coherence with rf fields, as explained above, but instead of NMR techniques to read-out the echo, optical techniques are used. As stated previously optical techniques are much more sensitive due to detector efficiencies which will give a better signal-to-noise ratio than NMR methods. In many cases the rf pulses are applied directly to the spin level, that is the coherence is established and rephased with rf. But in order to optically read out the result a beam is applied at the optical transition between levels B and C in figure 1.6 below. The optical field creates a coherence between the levels A and C, since there is already a coherence between A and B from the applied rf pulses. The output from the system is then two optical beams, the red and green, which beat against each other and giving a signal proportional to the NMR coherence.

A second method of establishing the coherence is with optical pulses, rather than rf, and

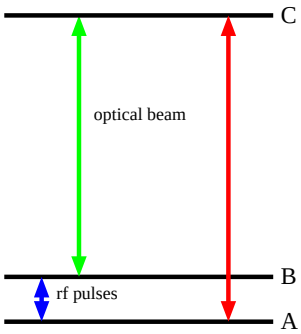

Figure 1.6: Pulses used in the Raman Heterodyne method.

this is also used in this work. This technique is known as the Raman method and was first shown in 1982, in an atomic thallium vapor [17]. Raman echoes have since been achieved in the $Pr^{3+} : Y_2SiO_5$ [18]. We have our standard 3 level system with the 2 spin levels and an optical level and in order to create an equivalent $\pi/2$ rf pulse two optical pulses are applied. First a $\pi/2$ optical pulse is applied resonant with the ground and excited state transition, this creates a superposition state between these two levels, then a π optical pulse is applied to the other optical transition, which pumps everything from the optical level into the excited nuclear spin level. The two optical pulses are equivalent to a $\pi/2$ pulse at the spin transition. The π pulse is much simpler to create, merely apply a π pulse

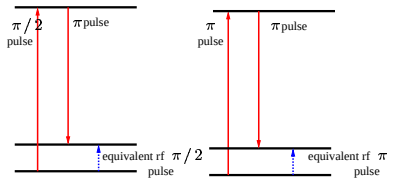

Figure 1.7: Raman $\pi/2$ pulse

at the two optical frequencies which is equivalent to a π pulse at the rf frequencies. This is illustrated in figure 1.7. In this case we again read-out the data optically by applying a read-out beam to the sample over the period of the echo, which creates the beat signal.

In the course of developing these techniques for studying the Pr-Pr interactions a number of other coherent transient measurements were performed. These were necessary to establish the correct experimental conditions or to discount certain effects in the interpolation of the data. These include photon echoes and spin nutation measurements. In the case of photon echoes we are measuring the coherence time of the optical level, which is much shorter than the spin state coherence time. Photon echoes were first seen in ruby in 1964 [19]. We have the simple 2-level system, though in this case the excited state is the optical level, rather than a nuclear spin level. The Hahn echo pulse sequence is used here as for spin echoes, though optical pulses are applied instead of rf ones. This pulse sequence creates the necessary coherence between the two levels and the one laser frequency supplies both the π and $\pi/2$ pulses. The detection method is still a heterodyne method.

Spin nutation is a measure of the Rabi frequency for the particular transition and it is caused by alternating stimulated emission and absorption by the sample as the system 'Rabi-flops' between the ground and excited states. The Rabi frequency for a particular transition depends on the intensity of the laser and the strength of the transition. Nutations are observed by switching on a driving rf field.

1.6 N-V Centre

The crystal I initially studied also satisfied the five criteria for a working quantum computer and it was also a solid-state system. In this case the optically active centre was the nitrogen-vacancy centre in a diamond. This centre is a substitutional nitrogen ion next to a vacancy in the carbon lattice and looks as in diagram 1.8. The N-V centre is, as with Pr^{3+}, a solid-state system and similarly the information is stored in the long-lived nuclear spin states. The level scheme of the N-V centre is as in figure 1.9 and as can be seen there is also an optical level in this case for read-out and manipulation of the spin states.

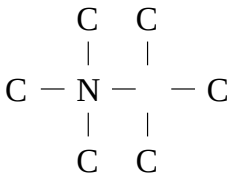

Figure 1.8: N-V Lattice

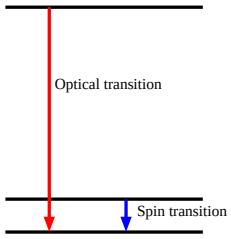

Figure 1.9: N-V Level Scheme

The coherence time in the case of the N-V centre is much shorter than the Pr^{3+} system, in this case it is of the order of 400μs [20], rather than the 82ms of Pr^{3+}. This means that any experiments on the interactions in Pr^{3+} will be more sensitive than those in the N-V centre. This higher sensitivity means that it is now possible to study smaller interactions, ones that haven't yet been studied.

The main difference between the Pr^{3+} and N-V centre is the dephasing mechanisms in the lattice. In the case of the N-V centre the lattice consists of carbon atoms which don't have a spin so that only other N-V centres or other impurities such as substitutional nitrogen ions are going to affect the dephasing. In the case of the rare-earth system though the Y ions do have a spin of 1/2 which means they will affect the dephasing of the Pr^{3+} ion.

Another difference is that the N-V centre has an electron spin of one and a nuclear spin of one as well. While the Pr^{3+} ion has no electron spin but has a larger nuclear spin of 5/2. The large electron spin of the N-V centre means that it is very sensitive to magnetic fields, since the magnetic moment of the electron spin is approximately 3 orders of magnitude larger than the nuclear spin magnetic moment. This means that the N-V centre is insensitive to the surrounding lattice, since there is no magnetic field produced by the carbon ions, but highly sensitive to the impurities in the system. The Pr^{3+} ion has an opposite effect where it is more sensitive to the surrounding lattice than the other impurities or Pr^{3+} ions. A final difference between the two systems is that the N-V has a much stronger optical oscillator strength. So in the N-V system any optical field will drive the centres much harder than in the Pr^{3+} system.

Some progress was made but major equipment failures led to this project being discontinued. The present program, however, has much in common in that again the main interest is in the perturbation of the coherence due to excitation of other centres in the crystal. A short account of the progress made in this N-V centre is given in the Appendix.

Theory

In this chapter will be discussing the reduced Hamiltonian for the spin ground states of the Pr^{3+} ion and how this is used to explain possible interactions. The strengths of the interactions between the Pr^{3+} ions and between the Pr^{3+} and Y ions will be estimated. The theory of the coherent transients will be presented and compared to the experimental results. The main method of determining the interaction strengths experimentally is to study the coherence time of the nuclear levels. The two methods used in measuring this time in this project will be numerically modeled. Initially I will be giving a theoretical description of spin echoes and in that sense will be looking at the 2-level system. I start with this reduced system because it is possible to obtain simple analytic solutions to this case as well as model it numerically, making it easier to debug. I will then move onto the full 3-level description of the system, with numerical simulations of the two different methods I used in experiments.

2.1 Ground State Spin Levels

The reduced Hamiltonian for the spin ground states of the Pr^{3+} ion is given by, [7]:

$$H = H_Q + H_{pQ} + H_Z + H_{nz} \tag{2.1}$$

where H_Q is the quadrupole Hamiltonian, H_{pQ} is the pseudo-quadrupole Hamiltonian H_Z is the electronic Zeeman interaction and H_{nz} is the nuclear Zeeman interaction. The quadrupole term represents the fact that the nucleus has a quadrupole moment. This term is sensitive to the electric field gradient of the nucleus and any change to this causes a change in the quadrupole splitting of the energy levels. The pseudo-quadrupole term is due to the fact that the nucleus of the Pr^{3+} has a magnetic moment while initially the electronic wavefunction has none. The nucleus' magnetic moment produces a magnetic field which induces a magnetic moment on the electronic wavefunction. This then acts back on the nucleus to produce an additional magnetic field there. The electronic Zeeman term is the enhanced magnetic effect, where the electronic wavefunction has an enhanced magnetic dipole moment when an external magnetic field is applied. This enhanced magnetic dipole moment than produces an enhanced magnetic field at the nucleus which results in linear Zeeman splitting. The nuclear Zeeman term is the splitting of the nucleus due to an applied magnetic field to the system.

The system appears as in figure 2.1.

The terms in the Hamiltonian have been determined and they can be written as:

$$H_Q + H_{pQ} = \mathbf{I} \cdot \mathbf{Q} \cdot \mathbf{I} \tag{2.2}$$

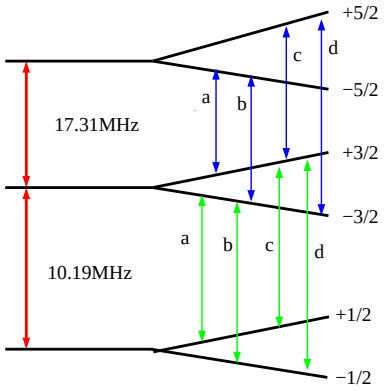

Figure 2.1: Level Scheme

$$H_Z + H_{nZ} = \mathbf{B^T} \cdot \mathbf{M} \cdot \mathbf{I} \tag{2.3}$$

where the **M** and **Q** are tensors, measured in MHz/G and MHz respectively, the **B** is the magnetic field and **I** is a 3×1 vector of spin matrices, where I = 5/2 in this case.

$$\mathbf{M} = \begin{bmatrix} 2.794 & -0.485 & -0.49 \\ -0.485 & 9.305 & 3.684 \\ -0.49 & 3.684 & 5.299 \end{bmatrix} \mathbf{/1000} \tag{2.4}$$

$$\mathbf{Q} = \begin{bmatrix} 0.353 & 0.234 & -0.372 \\ 0.234 & 3.403 & 1.978 \\ -0.372 & 1.978 & 0.688 \end{bmatrix} \tag{2.5}$$

The **M** and **Q** were obtained from [21] where spectra were recorded as a function of magnetic field magnitude and orientation. A full description of this can be found in reference [21]. From equations 2.2 and 2.3 we are able to find the energy levels for a particular applied magnetic field and hence find the transition frequencies. Besides determining these frequencies it is also possible to calculate the Rabi frequencies of these transitions which are proportional to their oscillator strengths. The Rabi frequency for a resonantly driven transition between the states $\langle g|$ and $|e\rangle$ is given by:

$$\Omega = \langle g|H_{int}|e\rangle/h \tag{2.6}$$

where $H_{int} = \mathbf{B_{rf}^T} \cdot \mathbf{M} \cdot \mathbf{I}$, in this case the magnetic field is given by the applied rf field.

2.2 Interactions

As discussed in the introduction there are three types of ion-ion interactions of interest: magnetic dipole-dipole, electric dipole-dipole and electric dipole-quadrupole. There are also three typical distances of interest, the Pr-Y, Pr-Pr under optical excitation and the Pr-Pr under rf excitation. The separation between Y ions in the lattice is simply $r_Y \approx 0.25nm$ [22]. The total concentration of Pr ions is 0.05%, or 5×10^{-4}, in my crystal. Since the optical linewidth of the crystal is 10GHz and the laser excited a 10Mhz spectral width, then the percentage of the optical line excited is 1×10^{-3}. Which means that the percentage

of Y sites occupied by an excited Pr^{3+} ion is 5×10^{-7}. The mean separation between optically excited Pr^{3+} ions is then given by:

$$\begin{aligned} r_{Pr} &\approx r_Y \times (5 \times 10^{-7})^{-\frac{1}{3}} && (2.7)\\ &\approx 0.25nm \times 170 && (2.8)\\ &\approx 30nm && (2.9) \end{aligned}$$

In the case of the rf excitation, all the Pr^{3+} ions are excited, so 100% of the optical line is excited. Using the equation 2.8 from above, the distance between rf excited Pr^{3+} ions is then 3nm.

2.2.1 Magnetic Dipole-Dipole

The Pr-Pr and Pr-Y interactions are both magnetic dipole-dipole interactions due to the spin states having a magnetic dipole moment. These different interaction strengths between the two ions are given by the following formula, ignoring any angular dependence:

$$f_{int} \approx \frac{\mu_0}{4\pi}\frac{\gamma_a\gamma_b\hbar}{r^3} \tag{2.10}$$

where the γ_a and γ_b are the interaction strengths of the different ions and the r is the distance between the two ions. When optically excited we have γ_{Pr} is 4kHz/G and r is 30nm, so $f_{Pr-Pr} \approx 60mHz$. The technique of Raman Heterodyne means that all the Pr^{3+} ions are spin flipped by the applied π pulse. At the concentrations I am dealing with this means that there is then a magnetic dipole-dipole interaction between Pr^{3+} ions only 3nm apart. At this distance the f_{Pr-Pr} interaction strength becomes 60Hz. Using the Raman Heterodyne method means that the resolution of any interaction strengths is then limited by this 60Hz, and we are unable to resolve any interactions that are smaller than this strength. If the Raman method is used though, this resolution will no longer depend on the Pr-Pr interaction. In this case the resolution is 60mHz, since optical excitation of the ions means the excited ions are further apart. The Y ion has a γ_Y of 210Hz and in this case the distance will be 0.5nm, which gives an interaction linewidth of $f_{Pr-Y} \approx 100kHz$. Hence the Pr-Y interaction is much greater than the Pr-Pr interaction, but the Pr-Y interaction can be turned off, making the Pr^{3+} ions insensitive to magnetic field changes to first order. This is done by performing the experiments at a particular magnetic field value and orientation [8]. At a field value of the order of 1kG there is a turning point in the transition energy levels. This field value must be correct to within a tens of G and within a few degrees, but it has been shown to give coherence times of 82ms.

2.2.2 Electric Dipole-Dipole

When a Pr^{3+} ion is optically excited it has a different electronic wavefunction which means that the electric field and electric field gradient felt by nearby Pr^{3+} ions also changes. Different electronic states have different electric dipole moments which is what causes this change. Now the electric field due to a dipole is given by:

$$E \approx \frac{1}{4\pi\epsilon_0}\frac{p}{r^3} \tag{2.11}$$

ignoring any angular dependence and p is the electric dipole moment. For Eu^{3+} we have that $p' = 34kHzV^{-1}cm$ [10] which becomes $2.3 \times 10^{-31}Cm$ after conversion. This value is expected to be similar to that of Pr^{3+} since they are both rare-earth ions. Using 30nm for the mean separation and the above value for the electric dipole it is possible to determine the electric field due to optical excitation of the Pr^{3+} ions, which is found to be $E = 77Vm^{-1}$. The electric dipole-dipole interaction is then given by: $\Delta f = E \times p/h$, which is 26.6kHz. This interaction is quite large and it is because of this that information stored in one ion is able to be transferred to surrounding ions.

2.2.3 Electric Dipole-Quadrupole

A rough estimate of the electric field gradient is given by:

$$\frac{\partial E}{\partial r} \approx 6\frac{p}{4\pi\epsilon_0}\frac{1}{r^4} \tag{2.12}$$

though $\frac{\partial E}{\partial r}$ is a 3×3 tensor this is only a rough estimate for the expected size of the different interactions. Using from above r = 30nm and p = 2.3×10^{-31} we then find that $\frac{\partial E}{\partial r} = 1.53 \times 10^{10}Vm^{-2}$. The nuclear quadrupole moment is $Q_{uad} = q \times 5.4 \times 10^{-30}Cm^2$, [23] where $q = 1.6 \times 10^{-19}$. The frequency shift due to the electric dipole-nuclear quadrupole interaction is given by:

$$f_{d-Q} \approx \frac{Q_{uad} \times \frac{\partial E}{\partial r}}{h} \tag{2.13}$$

$$\approx 20\mu Hz \tag{2.14}$$

All these calculations are just rough estimates, since we are only interested in orders of magnitudes for the different interaction strengths. It is possible that the electric dipole-quadrupole term is bigger than this due to the enhancement of the nuclear quadrupole moment, that we don't yet understand well. This term is so small it appears as if it should have no measurable effect on the spin states. At the moment we are not sure if the electronic electric dipole moment depends on the nuclear spin state. If this is true the optical excitation of ions will result in a linear Stark shift in the nuclear spin levels of surrounding ions. No theory exists on this since we are unsure as to whether there is a dependency of the electronic electric dipole moment on the nuclear spin levels.

2.3 Coherent Transient Techniques

2.3.1 2-Level System

Though the real system I am studying is in fact a 3-level system I will first focus on the simple two level scheme. In this case the two levels are just the nuclear spin levels used to store the information. I started with the simple 2 level calculations because they show the principles of spin echoes, which involve only 2 levels. This study was also a stepping-stone towards the more complicated 3-level scheme that more fully describes my system. The 2-level structure is easier to understand and debug before moving on to more complicated schemes.

2.3.2 Spin Echoes

I was interested in spin echoes in this project, which as explained before is the rephasing of coherence in the spin levels after a π pulse is applied to the transition. Before I could study the effects of any perturbations on the system it must first be possible to obtain a spin echo. Spin echoes form in a 2 level system, just the ground and excited nuclear spin levels, where rf pulses are applied between these two levels. Spin echoes are used to study the interactions between the ions because the resolution in this case is limited by the homogeneous width of the system, which is $1/\mathrm{T}_2$, and not the inhomogeneous width, of the order of 50kHz. In the study of spin echoes these is an ensemble of ions in an inhomogeneously broadened system, so this techniques allows us to go beyond this limit. The spin echo can reappear long after the coherence in the ensemble has disappeared so the delay times between the two rf pulses can be quite long. In this case we assume we are operating in the strong field limit for the pulses so the Rabi frequency is much larger than the inhomogeneous linewidth. The rf pulses are power-broadened due to this assumption, so all the ions in the ensemble are excited. In the following optical Bloch analysis the rotating wave approximation has been made. A full optical Bloch description of the spin echo can be found in [24].

The Bloch vector in this case is defined as:

$$\begin{aligned} \vec{R}' &= u'\hat{1}' + v'\hat{2}' + w'\hat{3}' && (2.15)\\ &= \vec{R} && (2.16) \end{aligned}$$

with components

$$u' = \rho_{12} + \rho_{21} \quad (2.17)$$

$$v' = i(\rho_{21} - \rho_{12}) \quad (2.18)$$

$$w' = \rho_{22} - \rho_{11} \quad (2.19)$$

There is another vector also defined, known as the pseudofield vector:

$$\vec{\beta} = |\chi^*_\omega(t)|\hat{1} + \Delta\hat{3} \quad (2.20)$$

where Δ is the detuning from resonance. In this case we have made the transformation to a rotating frame and so the components of $\vec{R}$ become:

$$u = u'cos\omega t + v'sin\omega t = 2Re(\rho_{21}e^{+i\omega t}) \quad (2.21)$$

$$v = -u'sin\omega t + v'cos\omega t = -2Im(\rho_{21}e^{+i\omega t}) \quad (2.22)$$

$$w = w' = \rho_{22} - \rho_{11} \quad (2.23)$$

where ω is the angular frequency the system is rotating at. With the system at thermal equilibrium the Bloch vector points downward along the $\hat{3}$ axis, since most of the population in the two-level system is in the ground state and there is no coherence. This means that $\rho_{21} \sim 0$ and $\rho_{22} \sim 0$, since ρ_{11} is the population in the ground level, ρ_{22} is the population in the excited level and ρ_{21} is the coherence between these levels. In this case

the Bloch vector is given by:

$$\vec{R_0} = \begin{bmatrix} 0 \\ 0 \\ -1 \end{bmatrix} \tag{2.24}$$

Which appears as in the figure 2.2 below. The generalized Rabi frequency is a value

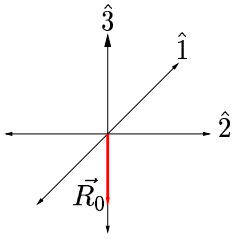

Figure 2.2: Initial Bloch Vector

which incorporates the detuning of the level and the normal Rabi frequency. It is given by $\chi = \sqrt{\chi_0^2 + \Delta^2}$. If the initial value of the Bloch vector is $\vec{R_0}$ and the generalized Rabi frequency is constant $\chi_\omega(t) = \chi_0$ then the value of the Bloch vector at a later time is given by:

$$\vec{R}(t) = \tilde{G}(t)\vec{R_0} \tag{2.25}$$

where:

$$\tilde{G}(t) = \begin{bmatrix} \frac{\chi_0^2 + \Delta^2 cos\beta t}{\beta^2} & -\frac{\Delta}{\beta} sin\beta t & \frac{\chi_0 \Delta}{\beta^2}(1 - cos\beta t) \\ \frac{\Delta}{\beta} sin\beta t & cos\beta t & -\frac{\chi_0}{\beta} sin\beta t \\ \frac{\Delta\chi_0}{\beta^2}(1 - cos\beta t) & \frac{\chi_0}{\beta} sin\beta t & \frac{\Delta^2 + \chi_0^2 cos\beta t}{\beta^2} \end{bmatrix} \tag{2.26}$$

In the case of a spin echo there is a $\pi/2$ pulse applied to the initial Bloch vector, $\vec{R_0}$. This pulse is a resonant pulse and it has amplitude χ_0 which is the Rabi frequency of the rf field applied. So the $\vec{\beta}$ vector than points along the $\hat{1}$ axis, since $\Delta = 0$. The $\vec{R}$ then precesses around $\vec{\beta}$ and to find the value of it after the $\pi/2$ pulse equation 2.25 is applied. A $\pi/2$ pulse is actually of length $t = \pi/2\chi_0$ and since $\Delta = 0$ and $\vec{\beta} = \chi_0\hat{1}$ during the pulse our $\tilde{G}(t)$ matrix that represents this pulse becomes:

$$\tilde{G}(\pi/2\chi_0) = \begin{bmatrix} 1 & 0 & 0 \\ 0 & 0 & -1 \\ 0 & 1 & 0 \end{bmatrix} \tag{2.27}$$

So after the $\pi/2$ pulse our $\vec{R}$ becomes:

$$\vec{R} = \begin{bmatrix} 0 \\ 1 \\ 0 \end{bmatrix} \tag{2.28}$$

which means the $\vec{R}$ points along the $\hat{2}$ axis and there is no population difference between $|1\rangle$ and $|2\rangle$ states. This system is then allowed to evolve and in that case the $\vec{\beta} = \Delta\hat{3}$, since there is no applied pulse and the system is undergoing free evolution. The Bloch

vector is then allowed to evolve for time t_1 so our $\tilde{G}(t)$ becomes:

$$\tilde{G}(t_1) = \begin{bmatrix} cos\Delta t_1 & -sin\Delta t_1 & 0 \\ sin\Delta t_1 & cos\Delta t_1 & 0 \\ 0 & 0 & 1 \end{bmatrix} \tag{2.29}$$

So our $\vec{R}$ is:

$$\vec{R} = \begin{bmatrix} -sin\Delta t_1 \\ cos\Delta t_1 \\ 0 \end{bmatrix} \tag{2.30}$$

Our $\vec{R}$ then rotates around the $\hat{3}$ axis, since each part of the ensemble has a different detuning they will rotate at different frequencies. After a time T_2^* the $\vec{R}$ are distributed over the 1-2 plane. At this time the vector sum $\vec{R_T}$ which corresponds to the radiating polarization density is zero. While at this time the ensemble has dephased, the subgroups with equal detuning evolve coherently. In the spin echo case there is then a π pulse applied to the ensemble. Similarly to the $\pi/2$ pulse the detuning can be ignored as this pulse is applied, since the pulses are short. The length of the pulse is $t = \pi/\chi_0$ and the amplitude is just χ_0. This results in:

$$\tilde{G}(\pi/\chi_0) = \begin{bmatrix} 1 & 0 & 0 \\ 0 & -1 & 0 \\ 0 & 0 & -1 \end{bmatrix} \tag{2.31}$$

This π pulse then has the effect of rotating each $\vec{R}$ for the different detuning through 180° about the $\hat{1}$ axis, so our $\vec{R}$ becomes:

$$\vec{R} = \begin{bmatrix} -sin\Delta t_1 \\ -cos\Delta t_1 \\ 0 \end{bmatrix} \tag{2.32}$$

If we now use the free evolution $\tilde{G}$ matrix, 2.29, from above we find that after a time t_1, equal to the time between the $\pi/2$ and π pulses, our $\vec{R}$ becomes:

$$\vec{R} = \begin{bmatrix} 0 \\ -1 \\ 0 \end{bmatrix} \tag{2.33}$$

Comparing the initial Bloch vector, 2.24, with the above vector, 2.33, we see that this Bloch vector is the same as the initial one, just 180° out of phase. The ensemble of ions have rephased and experimentally there should be an echo at this time. The amplitude of this rephasing is the same as that at the start due to the lack of relaxation terms in the analysis.

The Bloch vector at time $t_2 \neq t_1$ becomes instead:

$$\vec{R} = \begin{bmatrix} -cos\Delta t_2 sin\Delta t_1 + sin\Delta t_2 cos\Delta t_1 \\ -sin\Delta t_2 sin\Delta t_1 - cos\Delta t_2 cos\Delta t_1 \\ 0 \end{bmatrix} \tag{2.34}$$

This $\vec{R}$ is now integrated over the Gaussian linewidth of the detuning and so we obtain:

$$\vec{R} = \begin{bmatrix} 0 \\ -b \exp -\frac{(t_2 - t1)^2 b^2}{4} \\ 0 \end{bmatrix} \tag{2.35}$$

where the Gaussian linewidth is given by $g(\Delta) = \frac{1}{\sqrt{2}} \exp -\frac{\Delta^2}{b^2}$. If $\vec{R}$ is plotted out we find a delta function centered on the time t_1 which is the echo being rephased. This delta function reflects the fact that I used hard pulses to represent the π and $\pi/2$ pulses. We see that the ensemble has rephased, as we expected, at a time equal to the time between the two pulses. The echo amplitude will be the same as the initial amplitude, but 180° out of phase. There is no decay in the amplitude because I haven't included any relaxation terms, if these were included the echo would still be 180° out of phase, just the amplitude would be reduced. This shows that the spin echo method will always give an echo at the time after the π pulse which is equal to the time between the two pulses. This spin echo can be seen in the vector model in the figure 2.3 below. To see the effect of a perturbation

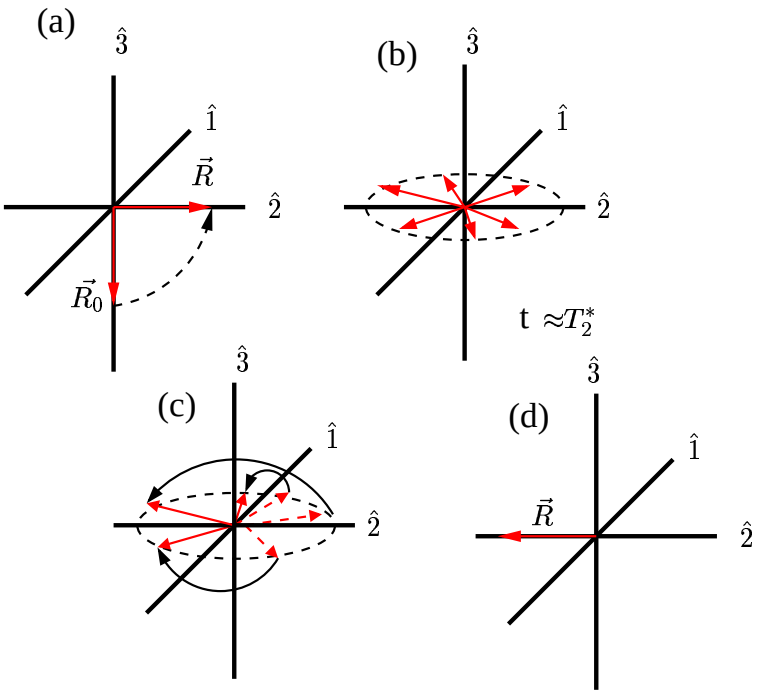

Figure 2.3: (a) The first pulse is applied to the ensemble and the spin states are then in a superposition state. (b) The ensemble begins to dephase at a rate related to their detuning and after time T_2^* the ensemble distributed in the 1-2 plane. (c)The π pulse flips the phase by 180° (d)The final Bloch vector that results, is the spin echo

on the system after the π pulse we simply change the detuning of the system to $\Delta' = \Delta + \delta$ after the pulse. So our $\tilde{G}(t)$ then becomes:

$$\tilde{G}(t) = \begin{bmatrix} cos\Delta' t & -sin\Delta' t & 0 \\ sin\Delta' t & cos\Delta' t & 0 \\ 0 & 0 & 1 \end{bmatrix} \tag{2.36}$$

So our $\vec{R}$ instead becomes:

$$\vec{R} = \begin{bmatrix} -cos\Delta' t sin\Delta t + cos\Delta t sin\Delta' t \\ -(sin\Delta' t sin\Delta t + cos\Delta' t cos\Delta t \\ 0 \end{bmatrix} \tag{2.37}$$

which simplifies to:

$$\vec{R} = \begin{bmatrix} sin\delta t \\ -cos\delta t \\ 0 \end{bmatrix} \tag{2.38}$$

If this detuning is simply a frequency shift to the whole ensemble then the only effect will be a phase change to the echo. If this detuning has a distribution of frequencies though, the echo will then be reduced due to the distribution of phases that will tend to cancel. These subgroups in the ensemble will still all rephase at the same time, they will just all have different phase shifts, so there is no longer constructive interference.

This spin echo can also be modeled numerically using matlab. In this case the rf pulses are modeled as in the optical Bloch derivation, that is they are instantaneous and affect the whole ensemble. From the above analysis we know that the $\pi/2$ pulse will take the system into a superposition state between the ground and excited nuclear spin states. This means the $\pi/2$ pulse acts on the level populations as follows; $|1\rangle \rightarrow \frac{1}{\sqrt{2}}(|1\rangle - |2\rangle)$ and similarly $|2\rangle \rightarrow \frac{1}{\sqrt{2}}(|1\rangle + |2\rangle)$. The matrix representing this pulse then appears as:

$$A = \frac{1}{\sqrt{2}} \begin{bmatrix} 1 & -1 \\ 1 & 1 \end{bmatrix} \tag{2.39}$$

For the π pulse though we have that the populations are inverted, so $|1\rangle \rightarrow |2\rangle$ and $|2\rangle \rightarrow |1\rangle$. In this case the matrix is:

$$B = \begin{bmatrix} 0 & 1 \\ 1 & 0 \end{bmatrix} \tag{2.40}$$

In this model it is simple to include relaxation terms, this means that the echo amplitude should decay as the delay time between the two pulses increases. In these numerical simulations of the echoes the relaxation terms are constants with respect to time. This is due to the fact that the interactions causing these relaxations aren't yet understood fully. We cannot yet make predictions as to how they will evolve with time and so are chosen as empirical constants. Detuning is also present in this model and is included in the excited nuclear spin level. The model is similar to the optical Bloch analysis in that the Rabi frequencies of the pulses are assumed to be much greater than the detuning and the pulses are short. During the pulses there is no relaxation because of this assumption. The relaxation terms, from [25], are given by:

$$\frac{d\rho}{dt} = \frac{\gamma}{2}(2\sigma^- \rho \sigma^+ - \sigma^+ \sigma^- \rho - \rho \sigma^+ \sigma^-) - \gamma_p[\sigma_z, [\sigma_z, \rho]] \tag{2.41}$$

The first bracketed term in this equation is due to spontaneous emission in the two-level system, while the second term is due to dephasing. Using these relaxation terms I was then able to model the spin echo in the two-level system and obtained the following plots, figure 2.4, from matlab. The upper two plots in figure 2.4, show that there is indeed

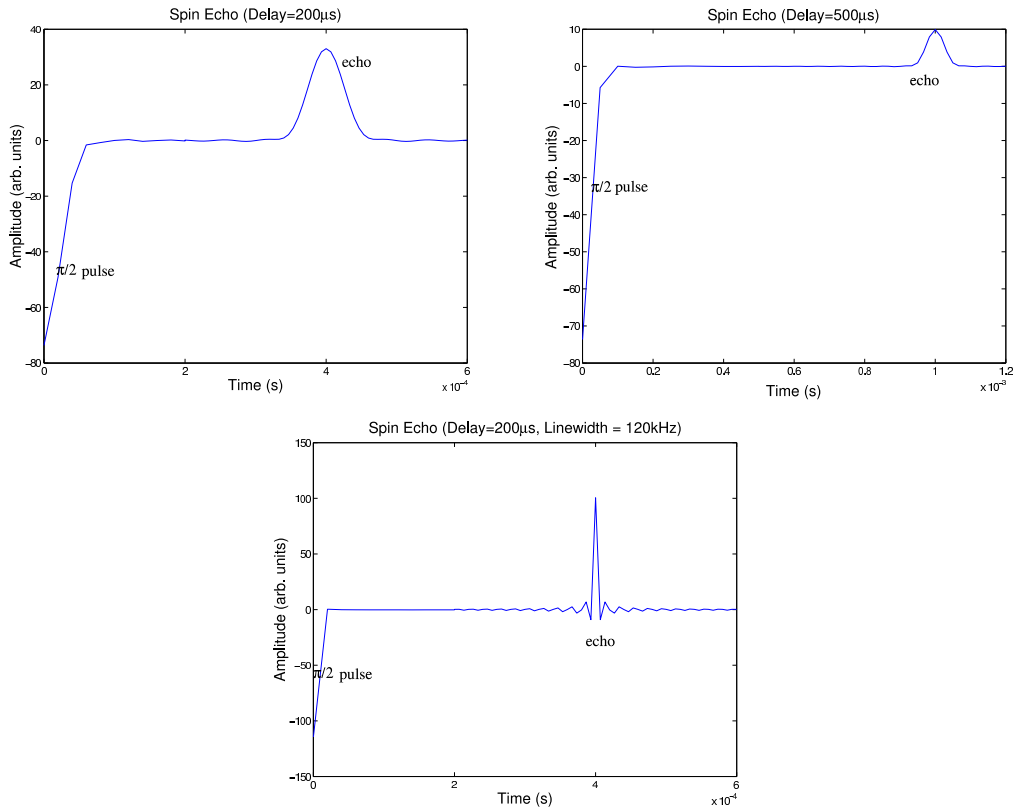

Figure 2.4: Spin echo plots

a spin echo formed from the rf pulses applied to the spin levels. The first plot is where t_1, the time between the $\pi/2$ and π pulses is 200μs while the second has a delay of 500μs. We see that the relaxation terms in this model are affecting the amplitude of the echo, that as the delay increases the amplitude decreases. We also see that as was shown in the optical Bloch analysis, the echo is 180° out of phase. In this case the echo isn't a delta function but this is due to the fact that the pulses are instantaneous while the linewidth of the detuning is 60kHz ($= \Delta$f), this means the echo duration will be $\sim 1/\Delta$f. In the lower plot we see, as expected, that an increased linewidth results in a decreased echo width. The numerical model of the system shows that there is a rephasing and hence an echo at the expected time. So from an analytic and numerical method it is seen that applying rf pulses to the spin levels creates coherence between these two levels. This coherence can be rephased through an rf π pulse to the sample.

As can be seen as the delay time between the two pulses is increased the echo amplitude also decreases. By plotting this decay against the t_1 it is possible to determine the time constant which is the coherence time of the system. The theory also shows that it is possible to have a coherence between the spin ground states through the application of rf π and $\pi/2$ pulses.

2.3.3 Photon Echoes

In order to achieve Raman echoes it must be possible to create coherence in the optical levels, which would manifest as a photon echo. The optical Bloch treatment is the same as for spin echoes [24], and it implies there is coherence generated. This optical Bloch method

uses hard pulses between the levels, but in reality we use soft pulses. Hard pulses are such that the Rabi frequency is assumed to be very much greater than the linewidth integrated over. In this case the width of the echo reflects the frequency width of the inhomogeneous line since they are instantaneous. While with soft pulses, the duration of the echo is related to the length of the pulses used. It is for this reason that the above models of the spin echoes showed a dependence on the inhomogeneous linewidth. When modeling in matlab, hard pulses are represented by matrices, these affect the entire population and are instantaneous. Soft pulses, on the other hand, are not instantaneous and they do not affect the entire population. In this case an on-resonant beam is applied to the optical transition and the Hamiltonian representing this is given by:

$$H = \Omega_1\sigma_{12} + \bar{\Omega}_1\sigma_{21} + \Delta\sigma_{11} \tag{2.42}$$

where the Ω_1 is the Rabi frequency of the applied optical pulse, which was chosen to be 100kHz and Δ is the detuning in the spin level, chosen as 200kHz. The above relaxation terms for the two-level atom were used, though in this case the empirical constants were chosen for the optical cases. As can be seen in the below numerical plot, figure 2.5, the soft optical pulses do create a coherence between the ground and excited optical levels. The use of soft optical pulses instead of the hard rf pulses that were used to create the

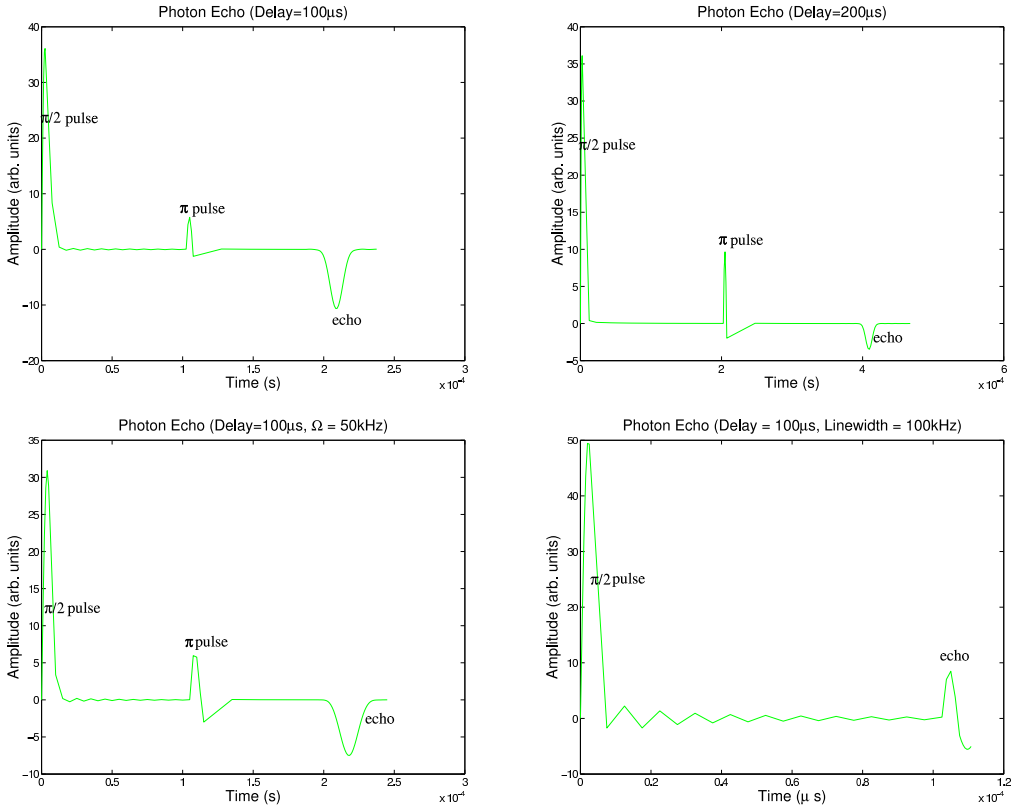

Figure 2.5: Photon Echo Simulations

spin echoes results in an echo that has a smaller amplitude than the spin echo case. This can be seen by comparing the amplitudes of figures 2.4 and 2.5 for the same delay times. The decrease in amplitude is caused because the soft optical pulses do not excite the entire ensemble. Only a subgroup of the ensemble is excited and so the number of ions rephased

by the π pulse, in the photon echo case, is less than that rephased by the hard π pulse of the spin echo case. In these plots the π pulse can be seen in the simulation which wasn't the case in the spin echo simulation. A perfect π pulse will create no new coherence between the levels, so it shouldn't be seen in the output. For this reason it wasn't seen in the output of the spin echo simulation. Photon echoes used soft pulses which means only the ions with zero detuning will experience a perfect π pulse. For this reason there will be subgroups of ions in the ensemble that create new coherence with the π pulse and so it is seen in the output.

When the pulses are longer it is seen that the echo width does increase as expected by the use of soft pulses. The lower left plot in figure 2.5 has a $\pi/2$ pulse length of 5μs, as opposed to the 2.5μs duration the two upper plots have. This is reflected in the wider echo of the lower left plot. The lower right plot shows that in the case of the soft pulses the echo shape does not depend on the inhomogeneous linewidth. The linewidth here is 100kHz as opposed to the 60kHz in the other simulations. As can be seen an alteration of the inhomogeneous linewidth has no effect on the echo shape.

2.3.4 3-level System

The system that I am studying isn't a 2-level system though, it is a three level system which makes the analysis more complicated and so the optical Bloch method cannot be used. The numerical analysis using matlab can still be performed though. Below, in figure 2.6, is a representation of the 3-level system. Where the γ_{ij}'s represent the decay of the

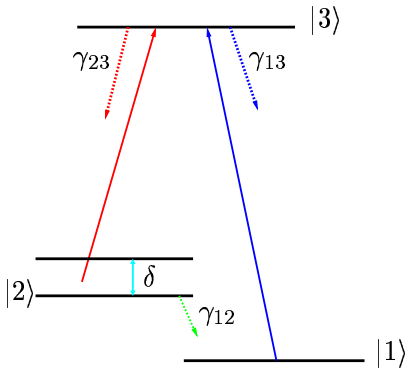

Figure 2.6: 3-Level System

coherence between the states $|i\rangle$ and $|j\rangle$.

In this case the relaxation terms, equation 2.41, are now the terms for the three level system and so are different from previous simulations. The relaxation terms though are still constant with respect to time as there can still be no prediction as to their time evolution. The terms present are the spontaneous emission term and the dephasing term. The spontaneous emission term is due to the fact that the excited ions will decay randomly from the optical level to the spin states. The dephasing term is due to other interactions in the system causing random perturbations to the energy levels and aren't yet fully understood.

The spontaneous emission term may be written as:

$$H = \frac{\gamma_{13}}{2}(2\sigma_{31}\rho\sigma_{13} - \sigma_{13}\sigma_{31}\rho - \rho\sigma_{13}\sigma_{31}) + \frac{\gamma_{23}}{2}(2\sigma_{32}\rho\sigma_{23} - \sigma_{23}\sigma_{32}\rho - \rho\sigma_{23}\sigma_{32}) + \frac{\gamma_{12}}{2}(2\sigma_{21}\rho\sigma_{12} - \sigma_{12}\sigma_{21}\rho - \rho\sigma_{12}\sigma_{21}) + \frac{\gamma_{12}N}{2}(2\sigma_{12}\rho\sigma_{21} - \sigma_{21}\sigma_{12}\rho - \rho\sigma_{21}\sigma_{12}) \tag{2.43}$$

The N in this equation is a measure of the temperature of the system and at low temperatures it can be taken as zero. The dephasing terms are as:

$$H = -\gamma_p[\sigma_z, [\sigma_z, \rho]] \tag{2.44}$$

In this case the σ_z is just the population difference between the two levels of interest. So the three terms are $\sigma_{11} - \sigma_{22}$, $\sigma_{11} - \sigma_{33}$ and $\sigma_{22} - \sigma_{33}$.

2.3.5 Raman Heterodyne Echoes

The Raman Heterodyne echoes are spin echoes, but here they are modeled in the full 3-level scheme. In this case there is also an optical read-out beam, which may have a perturbing effect on the ions. This three level system is first used to model the effect of a perturbing light field on the coherence. In this case the same hard rf $\pi/2$ and π pulses are applied to the spin levels to create the coherence and rephasing. Though in this case there is an additional resonant optical beam applied between $|2\rangle$ and $|3\rangle$ to mimic the effect of the read-out beam in the Raman Heterodyne experiments. This read-out beam is strong so it could have a perturbing effect on the resonant ions. From the below numerical simulations, figure 2.7, it is obvious that the read-out beam will effect the ions. In this case there are no spontaneous emission or dephasing terms and the Rabi frequency of the read-out beam is 100kHz, while the detuning is 200kHz and the inhomogeneous linewidth is 60kHz In the next set of figures, 2.8, there are relaxation terms included and the detuning, Rabi frequency and linewidth parameters are all as in figure 2.7. In figure 2.7, the Raman Heterodyne case with no relaxation included, the upper right plot is the case of the read-out beam on permanently. We see there is still an echo, just smaller in amplitude. When the read-out beam is pulsed on only over when the echo appears, lower plot in figure 2.7, then the amplitude is greater. The largest echo appears in the upper left plot, where there is no read-out beam. The second set of plots, in figure 2.8, shows that relaxation plays a large part in determining the shape of the echo. With no relaxation, figure 2.7, the echo amplitudes are larger, but more dispersive in shape, which is something we don't understand. With relaxation terms included, 2.8, the overall picture is the same, the amplitudes are just smaller in each case and the echoes don't have a dispersive shape.

The fact that this simulation is run in a three-level system has a large effect on the echo amplitude. Comparing the Raman Heterodyne echo with no read-out beam from figures 2.7 and 2.8, to the same delay in the spin echo case, figure 2.4 shows that the 2-level system has a larger echo. The three-level scheme has additional relaxation terms though, so it is to be expected that figure 2.8 gives smaller echoes. In the case of 2.7 though there are no relaxation terms included, so the smaller echo amplitude must be due to the fact that the simulation is run in a three-level system.

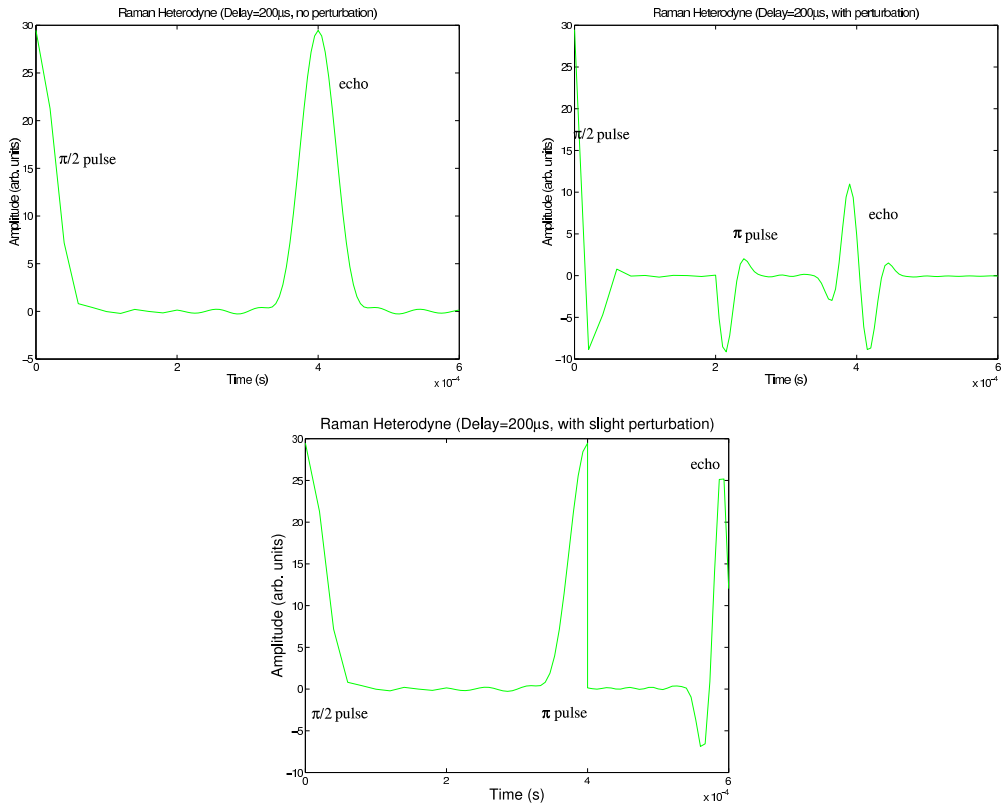

Figure 2.7: Raman Heterodyne Simulations: No Relaxation

2.3.6 Raman Echoes

Theoretically it has been shown that it is possible to create coherence in the optical levels using optical pulses, and coherence in the spin levels with hard rf pulses. In order to create a Raman Echo though it is necessary to create coherence in the spin levels using optical pulses. The Hamiltonian representing these soft optical pulses is the same as equation 2.42, though there are two beams used to create the coherence in the spin levels. There are then two Rabi frequencies which makes the Hamiltonian slightly more complicated. This Hamiltonian is given below:

$$H = \Omega_1\sigma_{13} + \bar{\Omega}_1\sigma_{31} + \Omega_2\sigma_{23} + \bar{\Omega}_2\sigma_{32} + \delta\sigma_{22} \tag{2.45}$$

In this case the Ω_1 and Ω_2 are the Rabi frequencies for the two optical transitions and the δ is the detuning in $|2\rangle$. This simulation is done in the full 3-level system with the dephasing and spontaneous emission contributions to the Hamiltonian.

This simulation was run twice, in the first instance the actual experiment was modeled with the pulses that were applied to the sample. As seen in figure 2.9, there is no coherence created in the spin levels from just straight optical pulses using the pulse sequence from our experiments. This model was then run again and instead of the second pulse sequence being as above, we used instead the sequence in figure 2.10. The extra π pulse should create more coherence between the spin levels and leave less population in the excited optical level. The maximum echo amplitude occurs when there is least population in the excited optical level since we have then pumped all the population into the spin levels. This optical pumping by the third π pulse means that any population left in the excited

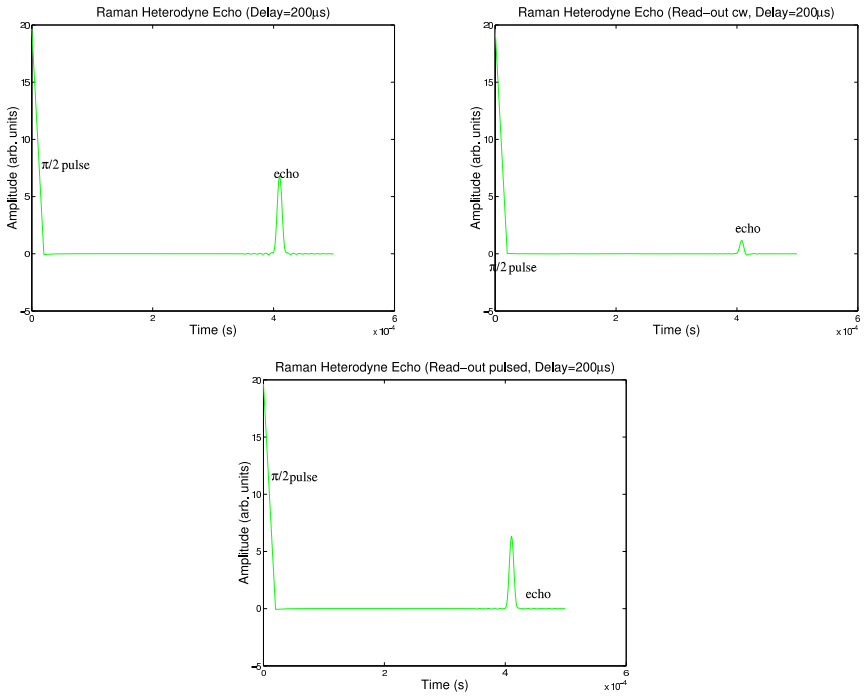

Figure 2.8: Raman Heterodyne Simulations: Relaxation

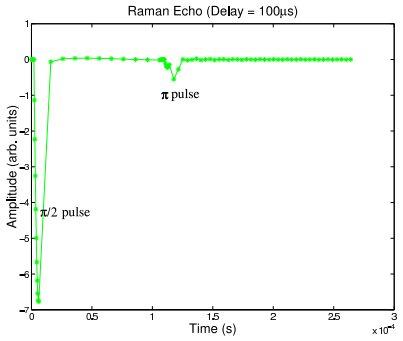

Figure 2.9: Raman Simulation: No Third π pulse

state is moved into the ground state levels, which gives the maximum coherence between these two. The first π pulse will shift everything from $|1\rangle$ to $|3\rangle$ and everything from $|3\rangle$ to $|1\rangle$. At the time of the π pulse there won't be much population left in $|3\rangle$ because it has such a short lifetime, 328μs, as mentioned previously. This means that after the first π pulse there will be a large population in $|3\rangle$ and not much in $|1\rangle$. This idea is presented in figure 2.11 When the second π pulse is applied it then transfers everything from $|2\rangle$ to $|3\rangle$ and vice versa. As before there should be a fairly large population in $|2\rangle$ so after the two π pulses there is still a significant population left in $|3\rangle$ and not much left in $|1\rangle$. This means that there is only a small coherence between $|1\rangle$ and $|2\rangle$. If a third π pulse is now applied between $|1\rangle$ and $|3\rangle$ then the small population in $|1\rangle$ is now in $|3\rangle$ and the large population that was in $|3\rangle$ is now in $|1\rangle$. This means that after the third π pulse we have maximum population in the two spin levels which means there will be a maximum coherence between the two which should give the largest possible echo amplitude. This pulse sequence gives what is an equivalent π pulse in the rf levels, as it is as if I have

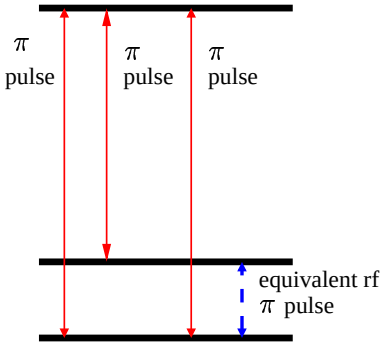

Figure 2.10: Optimal Pulse Sequence

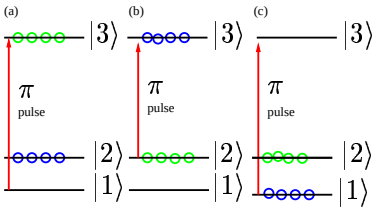

Figure 2.11: (a)After the first π-pulse there is population in $|2\rangle$ and $|3\rangle$ and none in $|1\rangle$.(b)Populations in $|2\rangle$ and $|3\rangle$ are inverted by the second π pulse. (c)Populations in $|1\rangle$ and $|3\rangle$ are inverted, leaving no population in $|3\rangle$ and the initial populations of $|1\rangle$ and $|2\rangle$ inverted

inverted the population of $|1\rangle$ and $|2\rangle$.

As can be seen in figure 2.12 the third π pulse creates a much bigger coherence, which shows in the relative echo sizes. In actually performing the experiment as I did, it would

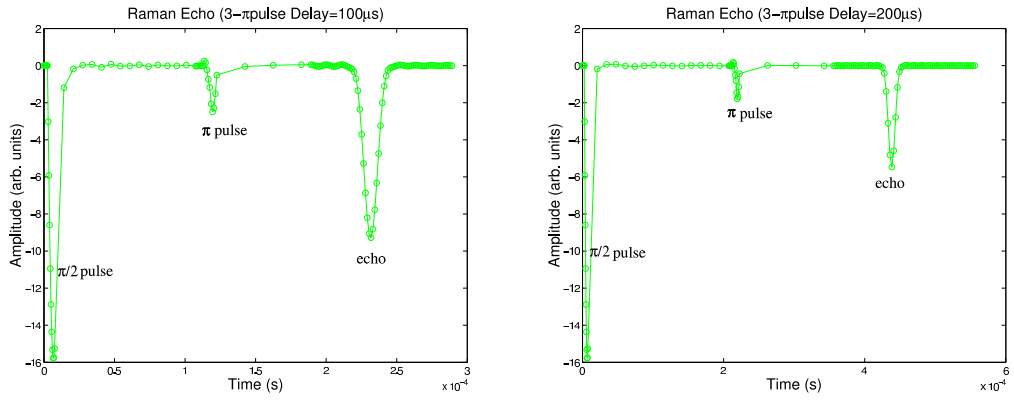

Figure 2.12: Raman echo simulations with optimal pulse sequence

be expected from the simulations that there should have been no echo at all. If the π and $\pi/2$ pulses had been exact then according to the theory we possibly would have produced no coherence. The fact that we did still see an echo was due to the fact that the $\pi/2$ and π pulses weren't exact. The laser instability would have also affected the echo amplitude and this instability is impossible to model. The simulation of the experiment shows no real insight into what is truly happening because of this instability. We had optimized the pulse areas in order to see some coherence, and they had been optimized to not be exact pulse areas.

Experiments and Results

3.1 Experimental Set-Up

For all the experiments performed the set-up was very similar. The main pieces of equipment used were the laser, cryostat and acousto-optic-modulators, (AOM's). The laser was a Coherent 699-29 ring dye laser, tuned to the $^3H_4$-$^1D_2$ transition at 605nm and frequency stabilised to 1MHz. It has the capability to be stabilised to sub-kHz, though this facility wasn't used in these experiments, in order to keep them simple. It was desirable to be able to scan the laser over ~200MHz, and if it was stabilised this couldn't be used. The slow scanning is purely a technique used to maintain a high concentration of optically active centres at the laser frequency. On the time scales of the experiment the laser can be thought of as at a fixed frequency.

The slow scanning of the laser combated any spectral hole-burning that would occur if the laser was at a fixed frequency. Spectral hole-burning occurs because the system is not a natural 3-level system and without scanning the laser bleaching would occur as the ions are optically pumped out of the states of interest. By scanning the laser the population distribution is rethermalised and bleaching does not occur. This spectral hole-burning can be overcome in other ways but this would complicate the experiment and so due to time-constraints couldn't be attempted.

The multiple beams at different frequency offsets that were required for the different experiments were achieved through the use of AOM's, which also allowed for pulsing of the beams. The sample was placed on a copper block, which was kept below 6K, inside a temperature variable cryostat. This low temperature was achieved using a liquid helium cryostat. Around the sample there was an rf coil and an orthogonal dc coil over the top. An electric field could also be supplied by applying a potential across the copper block and dc coil. The potential used in this case was 200V. The below schematic, figure 3.1, shows the set-up of the sample inside the cryostat.

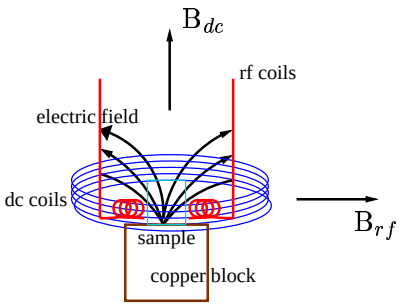

Figure 3.1: The laser beam is parallel with the B$_{rf}$

Figure 3.2, below, is a schematic of the experimental set-up.

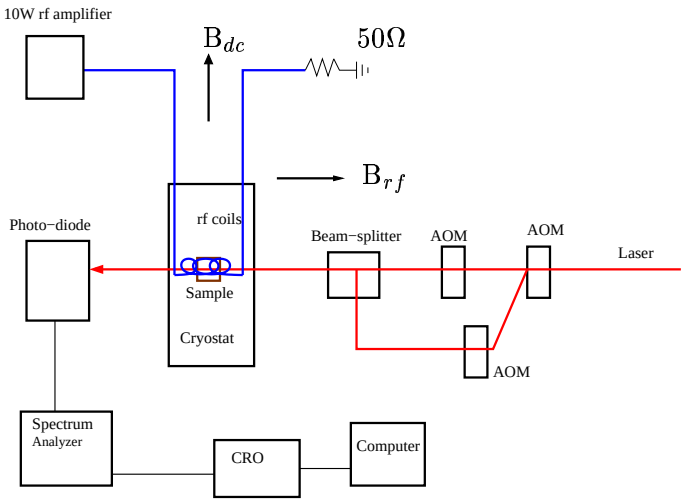

Figure 3.2: Experimental Set-Up

The laser beam was transmitted through the sample onto a photo-diode. The diode signal is then amplified before being fed into an analogue rf spectrum analyser. Recording was achieved by having the output of this spectrum analyser fed into a digital oscilloscope which was then averaged. A tracking generator ensured that the supplied rf was in sync with the spectrum analyser.

The dc and rf coils were calibrated with a hall probe. A number of different currents were supplied to the coils and the voltage was recorded, which was then able to be converted to give a magnetic field value.

3.2 Raman Heterodyne Spectrum

In this experiment the light is cw. The laser beam is transmitted through the sample and rf is supplied continuously via the rf coils. The frequency of the rf is scanned over 1MHz in the range of the $\pm\frac{1}{2} \rightarrow \pm\frac{3}{2}$ and $\pm\frac{3}{2} \rightarrow \pm\frac{5}{2}$ hyperfine transitions at ~10Mhz and ~17Mhz respectively. The rf excites the different transitions in this range and the Raman Heterodyne signal is recorded as a function of frequencies (see figures 3.3 and 3.6). When an external magnetic field is applied the levels split due to the Zeeman effect and the splitting increases as the field increases. Three different dc fields were used: 18.23G, 38.27G and 72.45G, all in the z-direction. Below, figure 3.3, are the spectra for these different values of magnetic fields: For a field in the z-direction there should be only 4 peaks, from the 4 transitions as seen in the level scheme, figure 3.4, with the transitions marked. There are instead 8 peaks which is due to the misalignment of the magnetic field. Due to the symmetry of the crystal there are two sites which are magnetically equivalent only if the field is orientated along the C_2 axis. Unfortunately if it is slightly misaligned or if there are residual non axial magnetic fields present then the two sites aren't magnetically equivalent. The two sites then split differently with the applied field and so the spectrum has 8 peaks instead of the expected 4. If an additional, non-axial (ie. not along the z-direction) magnetic field is also applied to the sample we see that the splitting between the pairs of peaks increases further figure 3.5. The additional magnetic field is introduced by a rare-earth magnet that is positioned outside the cryostat, near the

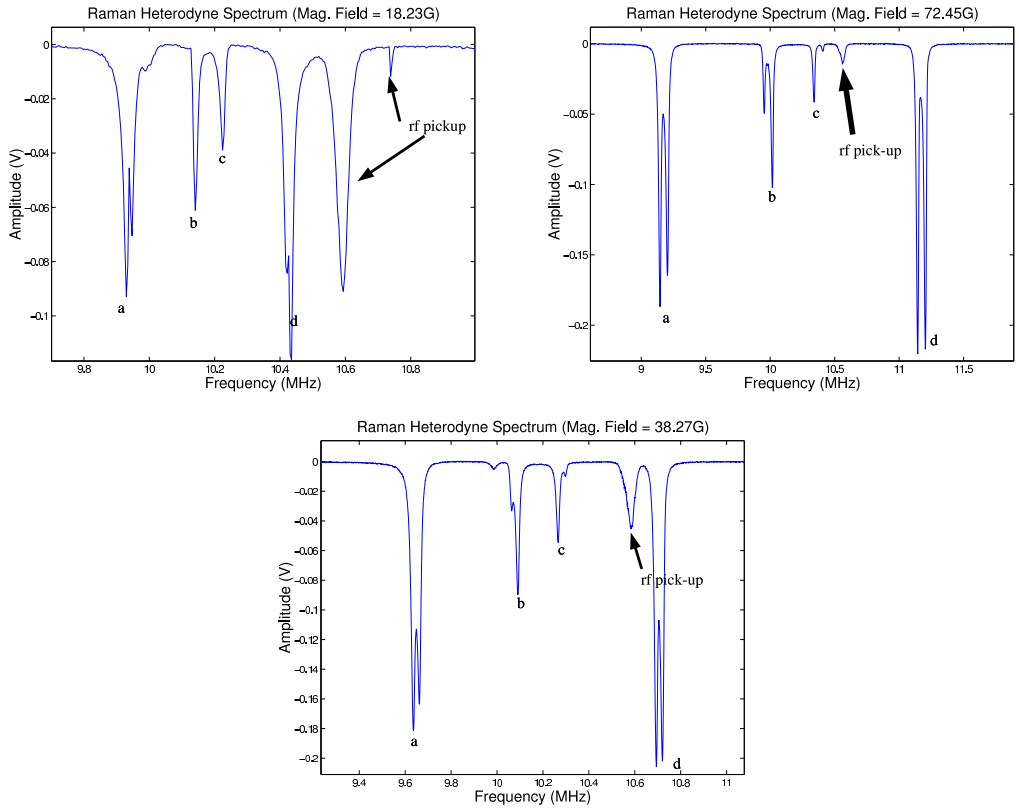

Figure 3.3: Spectra for different applied magnetic fields

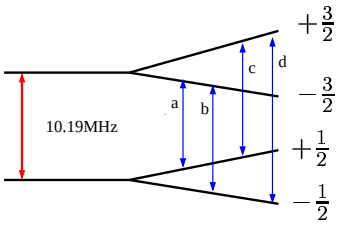

Figure 3.4: The transitions between the energy levels with a 72.45G applied magnetic field in the z-direction

sample. The dc magnetic field applied is just 18.23G and so from figure 3.5 it is easy to see the different transitions as well as the rf pick-up. Since the peaks due to rf pick-up are unaffected by magnetic field they remain stationary with the additional applied field. With the additional magnetic field the peaks split further, showing the magnetic inequivalency of the two ion sites. The experimental frequency of the transition corresponding to an axial field is determined by choosing the mean frequency of these two peaks.

In the level structure of the Pr ion there is another hyperfine level which also splits into two with an applied magnetic field along the z-direction. This level also has a spectrum as in figure 3.6. In this spectrum it is easy to see the 4 main transitions and the splitting due to the residual field interactions of the two magnetically inequivalent sites. The second peak is in fact two transitions that have interfered with each other to cause the unusual shape. In figure 3.7, the four main transitions that are seen in figure 3.6 are indicated.

The following table shows the experimental transition energies as compared to the theoretical ones obtained with the fitted free parameters for the different fields. For a

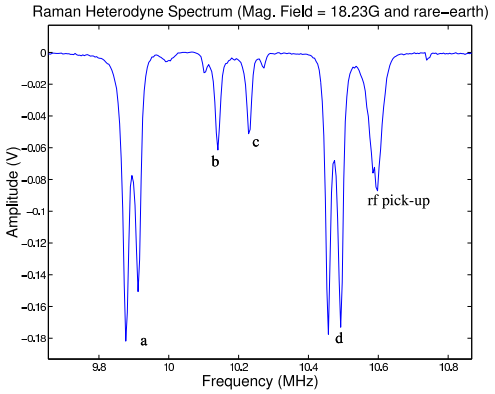

Figure 3.5: Spectrum of 18G field and rare-earth magnet

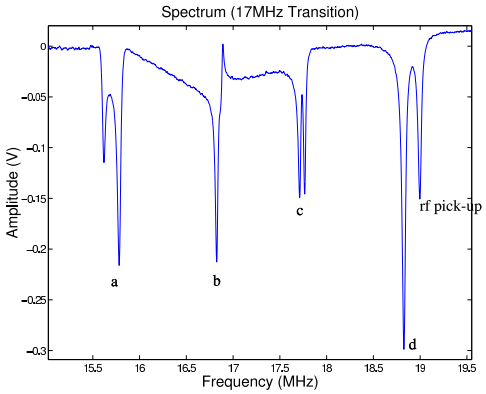

Figure 3.6: Spectrum of the 17MHz line transitions

detailed description of the fitted parameters see reference [21]. In this case we believe the field is along the z-axis, though there could be a very slight component along either the x- or y-axes. This is due to slight misalignment of the crystal and would be of the order of a few degrees. Tables 3.1, 3.2 and 3.3 are for the transitions from the 10MHz line, while table 3.4 is from the 17MHz line.

Experimental(MHz)	Theoretical(MHz)
10.6±0.1	10.44±0.08
10.4±0.1	10.23±0.02
10.2±0.1	10.15±0.02
9.9±0.1	9.93±0.04

Table 3.1: Transition Frequencies for 18.23G magnetic field

These tables show that the theory and experimental values are within error bounds of each other. The errors in the experimental values are due to the error in our ability to measure the centre frequencies and is not proportional to the magnetic field. In this case they are all determined to be 100kHz. The errors in the theoretical values are due to the misalignment of the field and the calibration of the dc coils. It was believed that the field was orientated along the z-direction, though there could have been a slight component in the x- or y-directions. This misalignment would have been of the order of $\pm 5°$. There was

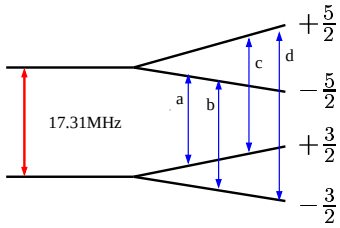

Figure 3.7: Transitions between energy levels, with an applied magnetic field of 72.45G in the z-direction

Experimental (MHz)	Theoretical (MHz)
10.7±0.1	10.73±0.08
10.3±0.1	10.28±0.04
10.1±0.1	10.1±0.03
9.7±0.1	9.66±0.07

Table 3.2: Transition Frequencies for 38.27G magnetic field

also an error from the calibration of the magnitude of this field, which was about 10%.

For the large magnetic field for both lines the values are the same to within two significant figures. The theoretical values are always within error bounds of the experimental values, but as the magnetic field is decreased the theoretical and experimental values don't agree as well as high magnetic field cases. This could be due to a residual field of ∼2G due to the magnetisation of the soft iron optical table, which would be more noticeable at low applied fields. The fit is relatively good and confirms the orientation of the crystal in the applied field.

3.3 Transition Strengths

The strength of the above hyperfine transitions is measured via spin nutation. The measurements are made in an applied dc magnetic field of 72.45G along the z-direction. The Raman Heterodyne signal was measured upon application of a 5ms rf pulse at the transition frequency. From the following examples, which are taken on the highest and lowest frequency transition on the 10MHz line, it is possible to see Rabi-flopping. The ensemble undergoes alternating absorption and emission as the ions are excited by the rf and then undergo stimulated emission to fall back into the ground state. The transition strength is proportional to the Rabi frequency of the transition. Below, figure 3.8, we see the nutation for the highest and lowest energy transitions.

The 17MHz transition also has nutation frequencies that are formed in the same way as the 10MHz transition and examples are shown in figure 3.9.

In the following experiments the $-\frac{1}{2} \rightarrow +\frac{3}{2}$, near 10MHz, transition was chosen, and

Experimental (MHz)	Theoretical (MHz)
11.2±0.1	11.21±0.15
10.4±0.1	10.38±0.08
10±0.1	10.03±0.07
9.2±0.1	9.2±0.14

Table 3.3: Transition Frequencies for 72.45G magnetic field

Experimental (MHz)	Theoretical (MHz)
18.9±0.1	18.93±0.3
17.7±0.1	17.75±0.08
16.9±0.1	16.86±0.09
15.7±0.1	15.68±0.3

Table 3.4: Transition Frequencies of 17MHz line at 72.45G magnetic field

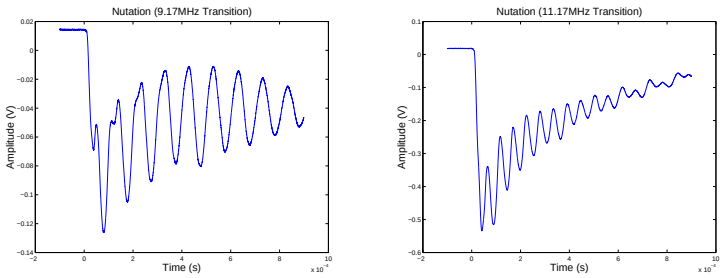

Figure 3.8: Rabi frequencies for the 10MHz line

the rf was set resonant with the highest frequency peak of 11.17MHz. This transition gave a high Rabi frequency which means it is a strong transition and should enable good echo signals. We saw in the theory section that hard pulses produced larger echoes than soft ones. In order to obtain good echoes experimentally it is necessary to have pulse lengths that are short with respect to the coherence time and in the current situation the pulses are approaching the ideal hard pulse. Larger Rabi frequencies mean that shorter pulses can be used, giving better echoes. In table 3.5 below, the labeled peaks are from the spectra in figure 3.3 and they have the following Rabi frequencies

Peak	Rabi Frequency (kHz)	Theory (kHz)	Δm
a	10.4	25.9±2.6	2
a'	16.6		2
b	3.3	13±2.4	1
b'	6.1		1
c	5.2	9.1±3.1	1
c'	1.9		1
d	8.3	22.8±1.9	2
d'	17.3		2

Table 3.5: Rabi Frequencies for the different transitions of the 10MHz line

The Rabi frequencies for the 17MHz line is in the table below,3.6 and the peaks are labeled from 3.6

The errors in the theoretical values are from the misalignment of the rf coil and from the errors in the calibration of the magnitude. The experimental and theoretical values do agree fairly well. There is only one theoretical value for each experimental pair of peaks since there should be little variation between pairs of peaks being associated with equivalent transitions. The experimental values could be different from the theoretical because if we are not resonant with a transition then we will be measuring the generalized Rabi frequency, which includes the detuning with the Rabi frequency. In order to obtain more accurate experimental values a better experiment would have been to find the generalized

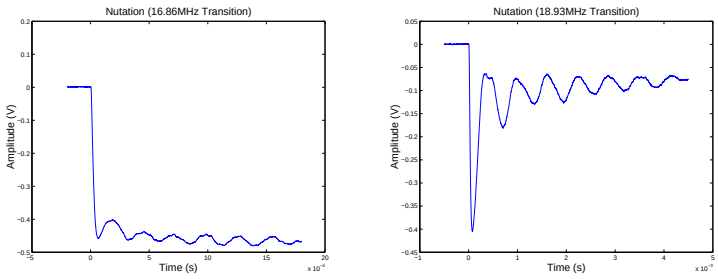

Figure 3.9: Rabi frequencies for the 17MHz line

Peak	Rabi Frequency (kHz)	Theoretical (kHz)	Δm
a	1.6	4.6±0.6	2
a'	1.6		2
b,b'	5	5.8±1	1
c'	3.7	6.9±1.5	1
d	1.4	4.2±0.6	2
d'	1.4		2

Table 3.6: Rabi Frequencies for the different transitions of the 17MHz line

Rabi frequency for a range of rf. As stated in the theory chapter:

$$\chi = \sqrt{\chi_0^2 + \Delta^2} \tag{3.1}$$

By plotting the generalized Rabi frequency for a range of detunings it is then possible to extrapolate and obtain the Rabi frequency of a transition.

It should be noted that the Rabi frequency is not directly proportional to the observed peak size in the spectra, as the transitions also involve population difference factors.

It is unknown why the peaks due to the residual field give two dissimilar values, particularly in the 10MHz line. Overall the $\pm\frac{1}{2} \rightarrow \pm\frac{3}{2}$ transitions are the stronger transitions and from this experiment it was easy to see on which transitions all echo experiments should be conducted.

From the above table 3.5, we see that, contrary to first order theory, it is generally the $\Delta m = 2$ transitions that are stronger. Mixing of the levels means that the quantum numbers, $\pm\frac{1}{2}, \pm\frac{3}{2}$ and $\pm\frac{5}{2}$, chosen to label the levels are no longer appropriate. The mixing doesn't seem to be as apparent in the 17MHz line transitions, since it is the $\Delta m = 1$ transitions that are stronger.

From these nutation it is then possible to find the approximate pulse areas for the $\pi/2$ and π pulses that need to be applied with the rf. The nutation oscillates at the Rabi frequency, so one period of the nutation is equivalent to a 2π pulse in duration. From this it is found that the π pulse was approximately 50μs long and so the $\pi/2$ pulse was approximately 25μs long.

3.4 Spin Echoes Experiment

3.4.1 Rf Echoes and Variation with Resonant Light Field and Magnetic Field

These experiments were conducted on the 11.17MHz transition, peak d' from table 3.5 since this has the highest Rabi frequency. From this frequency the pulse lengths were determined to be 25μs long and 50μs. The initial experiments creating Raman Heterodyne echoes were merely to optimize the conditions, to obtain the longest coherence time possible with the set-up. The pulse sequence in all these preliminary experiments were as follows: The

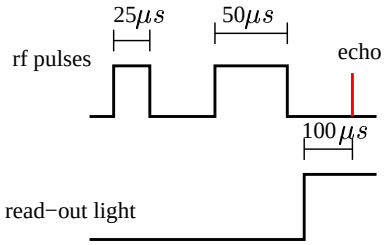

Figure 3.10: Pulse sequence for preliminary Raman Heterodyne experiments, times for delays and pulse lengths are marked

different conditions under which this was performed was at zero magnetic field, with a field and with the read-out beam pulsed and cw. In all these cases the set-up of the experiment was the same. There were two AOM's before the crystal, with a frequency difference of 10MHz. The beam then went through the crystal and on to the detector on the other side. The sample was mounted on a copper block inside a variable temperature cryostat with the temperature kept below 6K. The external magnetic field was applied through dc coils that surrounded the sample. The rf pulses were applied to an rf coil that was attached to the sample.

These different conditions all gave different coherence times which can be seen in the slopes of the below graph: For the optimized conditions the coherence time is (7.6±1.6)ms,

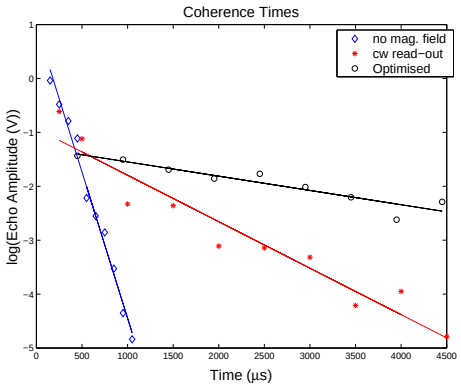

Figure 3.11: Raman Heterodyne Coherence Times

while with a cw read-out light this drops to (2.3±0.5)ms and if the magnetic field isn't on then the change is even more dramatic, falling to (370±35)μs, from the (7.66±1.6)ms time.

This lower coherence time in the absence of a magnetic field is due to the Y ions in

the lattice. In zero field the Y ions are all undergoing spin flips around the Pr ions which means that the Pr ions are all seeing a changing magnetic field from these flips, which will contribute to the coherence time. We indicate the effect of these different interactions in the following diagram, figure 3.12. The Pr-Y interaction strength is about 10-100Hz wide

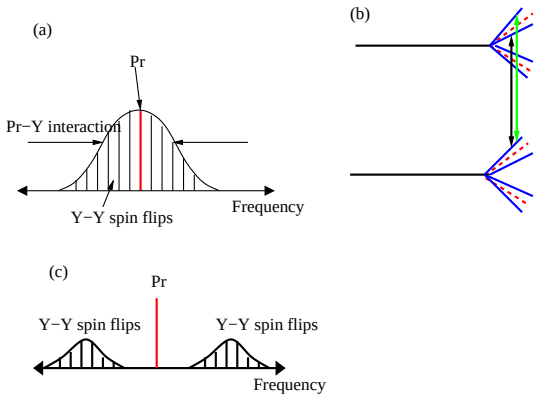

Figure 3.12: (a)Pr-Y magnetic dipole interaction (b) The energy level scheme for the coupled Pr-Y system (c) Pr-Y magnetic dipole interaction with applied magnetic field

which means that in zero field if the Pr ions are excited then all the Y ions are also excited. Figure 3.12 (b) shows the coupled Pr-Y energy level scheme, where the dashed red lines represent the Pr level scheme. The green arrow represents those transitions with no Y spin-flip, while the black arrow is a transition with a spin flip. As the applied magnetic field is increased the energy required to cause a spin flip increases due to the increasing Zeeman splitting. In frequency space, figure 3.12(c), the Y-Y interactions then move to increasing frequency, leaving the Pr ion alone in the centre. This means that when the Pr ion is optically excited the Y ions aren't. The Y ions then no longer have such a large changing magnetic field at the Pr site. This will then reduce the decoherence produced from the Y-Y interaction. A full discussion of this effect can be found in reference [26].

The cw read-out beam increases decoherence due to optical pumping because the optical levels have a much shorter coherence time than the spin levels. As the population is pumped into the optical levels it will then undergo spontaneous emission and relax into a random spin level. This process will rapidly destroy the coherence between the spin levels. For this reason the light is only turned on when it is actually needed, that is either to read-out the echo or to prepare the sample.

The coherence time wasn't critically temperature dependent because two sets of measurements were taken, one at 6K and another at 4K. In these cases the coherence times were(7.6 ± 1.6)ms and (6 ± 1)ms respectively, which are within error bounds of each other. Certainly in a solid it is unlikely that there will be longer coherence times at higher temperatures. Future experiments were all conducted within the above temperature range.

Below, figure 3.13, are plots of Raman Heterodyne Echoes taken at various delay times for the optimized case.

In this case the rf pulses are seen, but their amplitudes are less than the echo's. This is due to the fact that the read-out beam isn't on over the pulse sequence and the pulses are just rf pick-up from the detector.

The magnetic field in this case is at 72G and is supplied through the dc coils. If the echo measurements are now taken with no applied magnetic field we have the below plots, figure 3.14: Without the magnetic field the echo amplitudes decay much faster. The shape

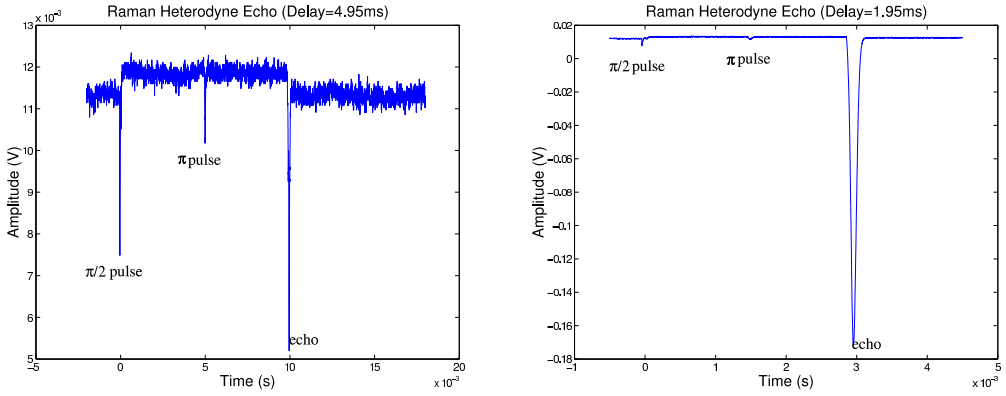

Figure 3.13: Raman Heterodyne Echoes for Various Delay Times

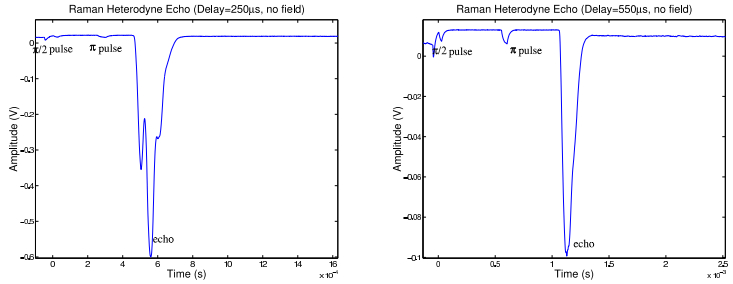

Figure 3.14: Raman Heterodyne Echoes with no Applied Magnetic Field

of the echoes is also different at nominally zero magnetic field for low delay times. This effect seems to disappear at around 500μs delay time. The unusual shape of the echo is believed to be due to a residual magnetic field still present that causes a slight splitting in the transitions. The rf pulses are then hitting both transitions which results in interference and the different echo shape.

If the read-out light is left on continuously but a magnetic field of 72G is applied in the z-direction then the following echo plot is obtained in figure 3.15:

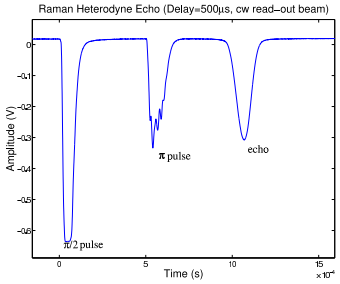

Figure 3.15: Raman Heterodyne Echoes with cw read-out light

Here we see that the rf pulses are much bigger than the echo, this is to be expected as in this case the light is on during the rf pulses. The detector can then see the Raman Heterodyne signal during the rf pulses, normally the rf pulses are only present due to rf pick-up of the detector. The rf $\pi/2$ pulse should be larger than the π pulse since it creates the coherence in the spin levels. The π pulse creates no new coherence, merely flips the

phase of the ensemble by 180° so in this situation it shouldn't be seen at all. The fact that it is observed, and in this case has the unusual shape, is likely to be due to the non-ideal pulse areas that are used in this experiment. Any inhomogeneities in the rf field will also contribute to the non-ideal case for the pulse areas and add to the different shape of the π pulse.

3.4.2 Perturbation of rf Echoes with a Second Light Field

In all the following experiments, unless otherwise stated, the read-out beam was pulsed and a magnetic field of 72G was applied to the sample in the z-direction.

With these optimized conditions off-resonant ions were optically excited with a second beam applied to the sample. This beam was created through the use of a second AOM and was detuned by 100MHz from the probe beam. The intensity of this beam was at a maximum of 10mW, while the read-out beam was less intense with only 4mW of power. The beams were combined before the sample on a beam-splitter and the results were collected using the same detector configuration.

The first experiment that was conducted with this set-up was with the below pulse sequence, figure **??**, where the off-resonant beam is switched on 50μs after the $\pi/2$ pulse has turned off, and turns off 200μs before the read-out beam is switched on. The coherence

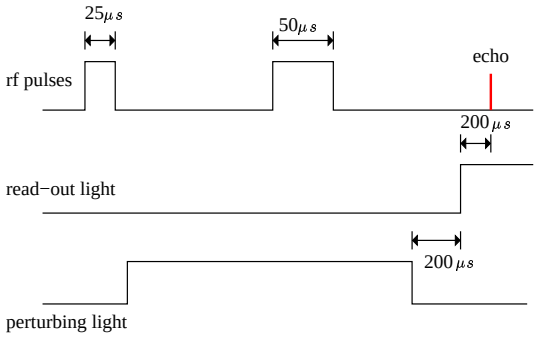

Figure 3.16: Experiment 1 pulse sequence

time for this experiment was measured as (4.7±0.5)ms, which is significantly lower than the (7.6±1.6)ms time for the unperturbed case. The second beam seems to be causing an uncontrolled interaction in the system, resulting in a decrease to the coherence time.

The next experiment that was performed with a cw second off-resonant beam. The coherence time in this case was slightly shorter at (4.3±0.4)ms.

Next the off-resonant beam was again pulsed, though this time it was also swept over ±5MHz, centered on the transition. The purpose of this scanning was to excite more off-resonant ions in the sample. In this case the beam came on as the π pulse turned off, and switched off 100μs before the read-out light was pulsed on, as seen in figure 3.17. Figure 3.18 show the π pulse followed by a transient and then the actual echo. This small transient can be seen in a number of different plots and it is due to the pulsing of the read-out beam. The coherence time here was longer than the two previous experiments at (5.0±0.5)ms.

Plotting the echo decay for these experiments along with the optimized Raman heterodyne case we see that the results are still inconclusive for the delay times, figure 3.19. Due to the scatter in the experiments the slopes appear the same over the delays measured. In this case it isn't possible to make any definite statement as to whether or not

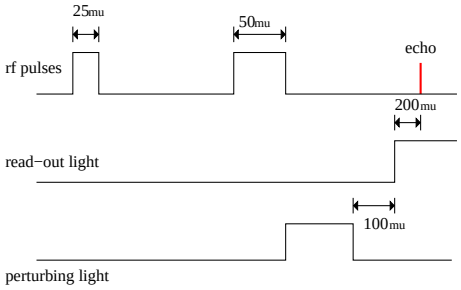

Figure 3.17: Experiment 3 pulse sequence

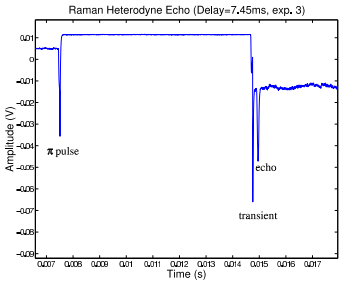

Figure 3.18: Raman Heterodyne Echo

the coherence time has been affected by these off-resonant ions. It is possible to determine an upper bound on the shift that could have possibly been seen. The Fourier transform of an exponential decay gives a Lorentzian curve with a FWHM given by $\frac{1}{\pi T_2}$. The FWHM of this Lorentzian is a measure of the shift to the energy levels from the perturbing beam.

$$\Delta\nu_{FWHM} = \frac{1}{\pi T_2} \tag{3.2}$$

Taking $T_2 = (4.74 \pm 0.5)ms$ we have that an upper limit to the shift is $\sim$40Hz. This shift is possibly due to the magnetic dipole-dipole, electric dipole-dipole or the electric dipole-quadrupole interactions. The most likely cause of this shift is the magnetic dipole-dipole interaction, though it is necessary to confirm the size of the electric dipole-dipole interaction.

3.5 Stark Effect

As discussed in the previous chapter one possible interaction affecting the spin states is an electric dipole-dipole interaction. For this interaction to be present it is necessary for the ion's electric dipole moment to depend on both its electronic and nuclear spin states. If this is the case then there should be a Stark shift on the nuclear spin transitions, given by:

$$\Delta\nu = \Delta p \cdot E \tag{3.3}$$

where Δp is the change in the electric dipole moment in going from one nuclear spin state to another. From this measurement and a knowledge of the optical Stark shift it is possible to determine the strength of the electric dipole-dipole interaction. It is possible to apply an external electric field significantly greater than the $80\mathrm{Vm}^{-1}$ estimate in the previous chapter, of the mean field changed by the ion due to its optical excitation. This

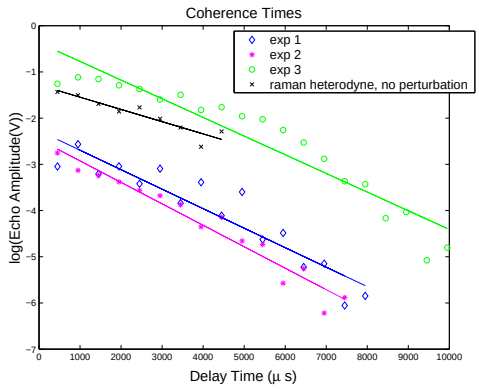

Figure 3.19: Coherence times for Raman Heterodyne echoes

experiment is then potentially more sensitive than the previous one. With this experiment there is only information provided on the electric dipole interaction and not about any quadrupole interaction as the field gradient due to the external field will be very small. This high electric field is supplied to the sample through the use of a high voltage pulse.

The high voltage pulse, of 200V, was applied to the sample, over the π pulse and the time at which the echo should appear in order to measure the Stark shift of the nuclear spin states. A similar experiment was performed by Meixner et al [10] in 1992. This group measured the Stark shift on the electronic level in Eu^{3+} which is similar to the experiment we performed. This voltage is applied across a distance of about 1cm so the total change to the electric field is $\sim$10kVm^{-1}. The electric field change across the sample is assumed to be 10% of this since the sample is $\sim$4mm, so the change in the electric field across this is then of the order of 1000Vm^{-1}. The idea behind this applied electric field is to mimic the change in the electric field caused by the optical excitation of off-resonant Pr ions. In the previous experiment the change in the electric field through this optical excitation is of the order of 80Vm^{-1}. My applied high voltage pulse provides a change in the electric field an order of magnitude larger than that from the optical excitation.

This high voltage pulse switched on as the π pulse switched off and turned off 50μs before the read-out light came on. This is shown in the below pulse sequence, figure 3.20.

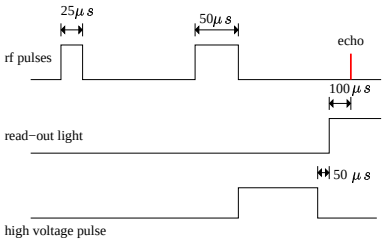

Figure 3.20: Stark shift experiment pulse sequence

This pulse was applied to the copper block that the sample was mounted on and was such that it was very inhomogeneous across the sample. The ground was the dc coils surrounding the sample and the change in the electric field was quite large across the sample. The electric field was applied to the copper mount so on the atomic level the change in the electric field gradient was vanishingly small so it is the electric dipole-dipole interaction measured, not the electric dipole-quadrupole one. Hence the experimental

set-up is as in figure 3.21.

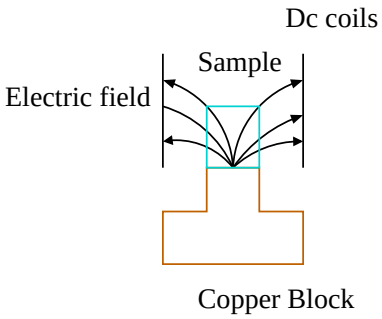

Figure 3.21: Stark Shift set-up

Comparing the plots of the echo amplitudes for the Stark effect and the optimized Raman Heterodyne case we see that the slopes are fairly similar and in fact the coherence time for the Stark Effect is (5.6±1.1)ms which is almost with error bounds of the optimized case. No conclusive statement is able to be made as to whether or not there has been an effect here. If there is an effect it appears to be quite small. Figure 3.22 shows the coherence time for the Stark Effect compared to the normal Raman Heterodyne echoes.

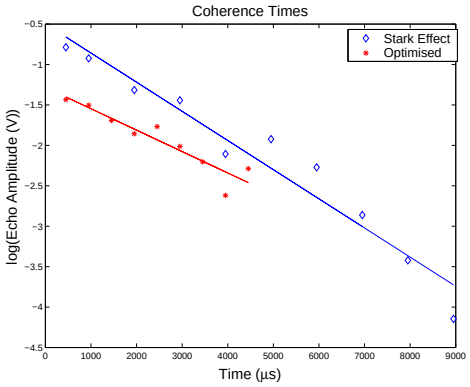

Figure 3.22: Stark Effect Coherence Times

The resolution of this experiment puts an upper bound on the interaction strength of 23Hz. From equation 3.3 above we see that the biggest change to the electric dipole moment from the spin states is then 23mHzV^{-1}m.

3.6 Raman Echoes

Before attempting to create Raman echoes there were a few preliminary experiments performed, creating Photon echoes and Pseudo-Raman echoes.

3.6.1 Photon Echoes

Photon echoes are created through the application of $\pi/2$ and π pulses to the optical transition. The beam through the sample was pulsed, with pulses of length 2μs and 4μs and was shifted from the laser frequency by 80MHz through the use of an AOM. There was another beam through the sample that was shifted by 82MHz and is only on during the read-out, so the echo was observed as a 2MHz beat on the detector. The pulse sequence

for this experiment is as in figure 3.23. In figure 3.24, the coherence times for the two cases

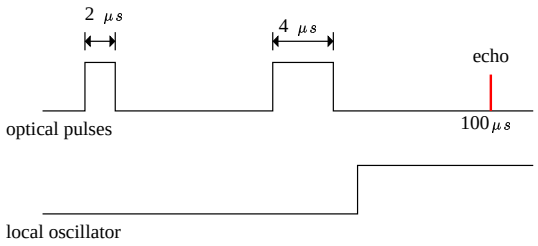

Figure 3.23: Photon echo pulse sequence

is compared. The actual coherence times for the two echoes are (120±15)μs for the photon

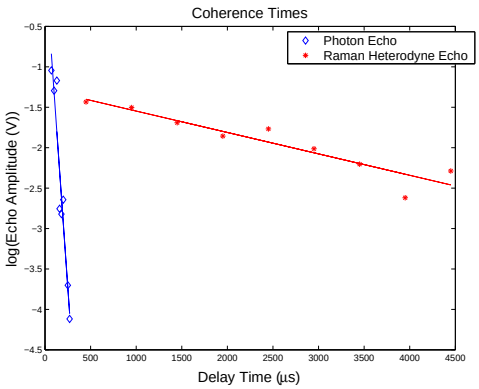

Figure 3.24: Coherence Times for Photon and Raman Heterodyne Echoes

echo and as previous, (7.6±1.6)ms for the Raman Heterodyne case. The coherence time for the optical level is shorter than that obtained by other groups, [9]. One reason for this is variations in the different samples used. The optical level has a vastly smaller coherence time than the spin levels do. Hence when performing the Raman Echo experiment delay times greater than 500μs will give Raman echoes and not photon echoes.

3.6.2 Pseudo-Raman Echoes

This experiment was devised to test if coherence could be generated in the spin levels with optical pulses and was only a preliminary experiment to the Raman echoes one. Two optical pulses are applied to the experiment at the two optical frequencies in the system. One is a $\pi/2$ pulse and the other is nominally a π pulse which is in order to create an equivalent rf $\pi/2$ pulse. An rf π pulse is then applied to the spin levels to create the pseudo-Raman echo. This pulse sequence is seen in figure 3.25. In this case instead of the

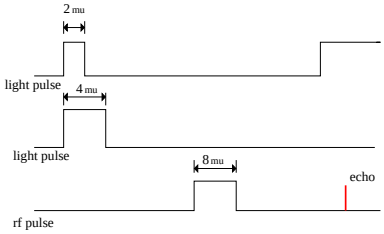

Figure 3.25: Pseudo-Raman pulse sequence

usual 10W rf amplifier a 200W amplifier was used. The pulse duration in this case has then been optimized to compensate for the additional power and it is 8μs instead of the 50μs. This 200W amplifier was used instead because the spin levels needed to be hit hard to ensure all the coherence generated is rephased and to allow the pulse to be short, so closer to the theoretical idea of a hard pulse.

The set-up for this experiment is slightly more complicated than the straight spin echo case. Since the coherence is being generated optically there was two beams of different frequency and these must be mode-matched. This is the case because the two beams need to be exciting the same group of ions in order to create the coherence. These beams were mode-matched by ensuring that their path-length was the same and that they were overlapped on the crystal and beam-splitter.

Optimizing the optical pulses is done by not only varying the length of the pulses, but also varying the intensity of the two beams. The optimal case was found to be when both beams were approximately 6mW in power and the $\pi/2$ pulse is 2μs long. From the below echo plot, figure 3.26, we see a pseudo-Raman echo.

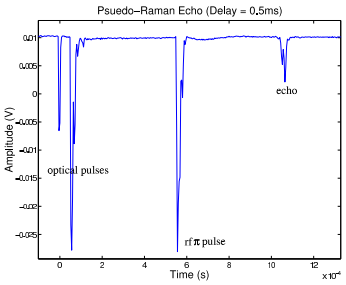

Figure 3.26: Pseudo-Raman Echoes

These echoes are not photon echoes, since in this case the delay times are such that we are beyond the regime for photon echoes. These must be some other echo, called pseudo-Raman echoes since they involve a hybrid scheme.

Note that the above pulse scheme has been used to obtain what has been claimed to be slow light in a solid in a recent Physical Review Letters article [27]. Here the light pulse has been delayed a factor of five times longer than given in that work.

Raman Echoes

Raman echoes are generated with a fully optical experiment no rf pulses are used to rephase or create the coherence. The pulse sequence for this experiment is as in figure 3.27. In this

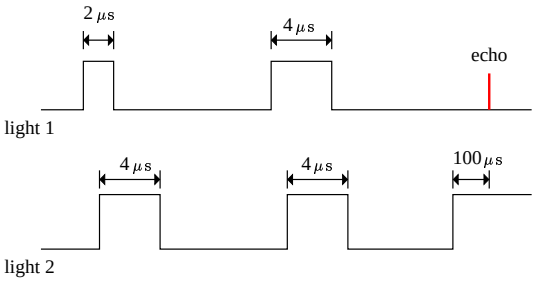

Figure 3.27: Raman pulse sequence

case one beam is switched on 2μs before the other, where this order was optimized, since

it was found that the ordering of the pulses was important. The less intense beam should be switched on after the other one, which is more evidence that I did produce Raman echoes. One of the beams was used as an optical pump and if the order was switched the population differences were not correct and so the echo was diminished. The coherence time for this Raman experiment was (2.5±0.6)ms, which compares with a coherence time of (4.2±0.8)ms from the Raman Heterodyne method. The fact that a shorter time was recorded with the Raman method will be discussed in the next chapter. Below is a plot of the first Raman echo obtained in our lab, and the first time this experiment has been done in an applied magnetic field, figure 3.28. The latter is significant given the longer coherence times obtained when operating in a field.

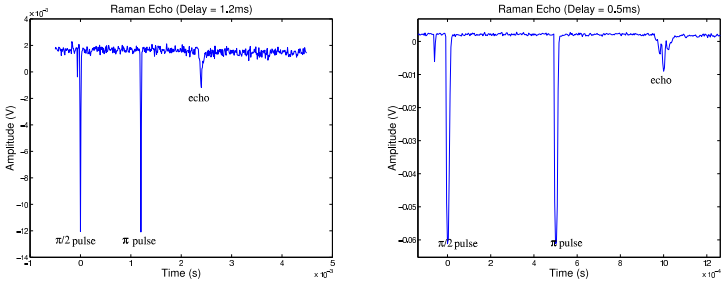

Figure 3.28: Raman Echoes

Below, figure 3.29 is a plot of the coherence times for the Raman and the Raman heterodyne cases.

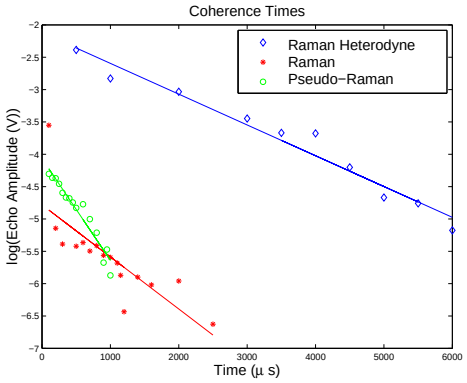

Figure 3.29: Coherence Times for Raman, Pseudo-Raman and Raman Heterodyne Methods

Discussion

4.1 Raman Heterodyne Echo Perturbation with Light and Rf

This set of experiments investigated whether optical excitation of off-resonant ions perturbs the nuclear spin states of the on-resonant ions. In a quantum computer information is stored in the ground state nuclear spin levels, which are the spin qubits. If a gate operation, or optical excitation of an ion, is performed on an electronic qubit in the vicinity of these spin qubits, will this affect the stored information?

The expectation was that the perturbing beam would decrease the coherence time. From graph 3.19 it was possible to determine an upper bound on the interaction strength, from the uncertainties in the measurements, to be $\sim$40Hz. However changes are all below the level of errors and so in order to make a more definite statement as to the effect of this second beam this experiment must be repeated with improved sensitivity. Performing the experiment at the specific magnetic field and orientation discussed previously is one such method. This specific magnetic field will increase the coherence time from 7ms to 80ms, which is a ten-fold improvement in sensitivity. As discussed in Chapter 2 one possible ion-ion interaction affecting the spin states is an electric dipole-dipole interaction. For this interaction to be present it is necessary for the ion's electric dipole moment to depend not just on its electronic state, but also its nuclear state. An attempt was made to obtain an estimate of the size of this effect.

The experiment was performed in order to determine if there was an electric dipole moment associated with the ground state spin levels. The Stark effect is a shifting in the energy levels due to an electric field. A high voltage pulse was applied after the π pulse, hence the evolution will not be symmetric about the π pulse. If the change in the electric field caused an effect on the Pr^{3+} ions, this experiment should destroy the echo. Instead a similar coherence time was seen which was within error bounds of the unperturbed case. The upper bound of the Stark shift to the nuclear spin levels that would have been undetectable with the current resolution is 23Hz. Whilst an upper bound for the change to the electric dipole moment from the nuclear spin states is 23mHzV^{-1}. Optical excitation of off-resonant Pr^{3+} ions produces a mean field of the order of 80Vm^{-1} at the on-resonant Pr^{3+} ion site. From equation 3.3, there is then an upper limit of approximately 2Hz on the Stark shift to the nuclear spin states from this mean field. This Stark shift to the spin levels is much smaller than the resolution of the Raman Heterodyne experiment with the perturbing beam, and so for this reason we wouldn't have been able to detect any electric dipole-dipole interactions due to optical excitation.

This experiment needs to be more sensitive before this possible Stark shift in the nuclear spin states can be measured. It is achievable for us to improve the sensitivity

by two orders of magnitude which should be enough for us to then directly measure any interaction with the perturbing beam. One improvement is to perform the experiment at the specific magnetic field discussed in previous chapters. T_2 then improves by one order of magnitude, changing from 5ms to 80ms. Another order of magnitude of sensitivity is gained through the use of phase sensitive detection. This form of detection means that it is the value of the electric field that is studied, not the variation in it. We were able to apply an electric field of 10kVm^{-1}, so this is used instead of the electric field change across the sample which was 1kVm^{-1}. In order to improve the shot-to-shot noise we can stabilise the laser to ~100Hz.

In the experiment was established a probable change to the decoherence of the nuclear spin levels, which is seen in a shift to these levels, of the order of 40Hz. The origin of this shift has not yet been determined, though it is probably not all due to the electric dipole-dipole interaction. The thought is that it was mainly caused by the magnetic dipole-dipole interaction, though the size of the electric dipole-quadrupole interaction has not yet been determined experimentally. The consequence of this 40Hz shift to the nuclear spin levels in the operation of a quantum computer is the number of gate operations that can be performed with the system before stored information is lost. From previous chapters we know the electric dipole-dipole interaction of the optical levels gives a shift of $\Delta\nu_{optical} = 26kHz$ to the optical level. Optically exciting one ion causes a Stark shift in the optical levels of 26kHz in a nearby ion. From the above discussion we know this optical excitation causes a shift in the spin levels of not more than 40Hz. Our quality factor is:

$$Q = \frac{\Delta\nu_{optical}}{\Delta\nu_{spin}} \tag{4.1}$$

$$= 650 \tag{4.2}$$

which is a high quality factor. This implies that the phase error is then quite small, allowing time for many gate operations before information is lost. Now

$$phaseerror = \frac{360^\circ}{Q} \tag{4.3}$$

$$= 0.5^\circ \tag{4.4}$$

The phase error, in degrees, obtained after one gate operation is, 0.5°. This means is is possible to perform about 100 gate operations on nearby qubits before there is a 180° phase error in the nuclear spin states. The interaction size, regardless of its origin, means it is possible to perform almost 100 gate operations before the information is lost.

4.2 Raman Echoes

In the proposed rare earth quantum computing situation it is necessary to obtain coherence in different subsets of ions. The subsets are selected optically and hence the coherence must be generated using an optical technique. For this reason it is necessary to be able to create Raman echoes, here the nuclear spin level coherence is created with optical pulses. These Raman echoes were the first time they had been achieved in our lab. It is also the first time that Raman echoes have ever been produced in Pr^{3+} ions in a magnetic field. From these echoes it was possible to investigate whether excitation of the ions with rf was different from optical excitation.

When the rf pulses are applied to the sample all the ions are being driven in the same way. When optical pulses are applied though only a subgroup of the ions are affected by the light. This is due to the fact that the inhomogeneously broadened spin levels have a narrower linewidth than the inhomogeneously broadened optical levels. The linewidth of the spin transitions is of the order of 100Hz, whilst the optical level has a linewidth of 1GHz. The rf-field is power broadened and so it is wider than the inhomogeneous linewidth of the spin levels. Hence any rf pulse applied to the sample is seen by all the ions. The linewidth of the applied laser is at most 1MHz, so only 0.1% of the Pr^{3+} ions will be affected by optical pulses. This is seen in the below diagram, 4.1: The Raman Heterodyne

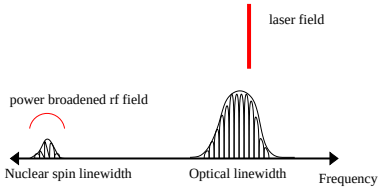

Figure 4.1: Inhomogeneous linewidths of the spin and optical transitions

method uses rf pulses to create the coherence in the spin levels. All the Pr^{3+} ions are excited by these pulses and so there are large magnetic field fluctuations, dephasing the subgroup producing the echo. For this reason it was thought that the coherence time would be longer when measured with the Raman technique over the Raman Heterodyne, since the Raman only excites 0.1% of the Pr^{3+} ions. Instead though the Raman method gave a shorter time, (2.5±0.6)ms as opposed to (4.2±0.8)ms. The shorter coherence time is probably due to the laser instability as argued below.

In both methods the laser is on for a long time leading to a large hole being burnt, of the order of 10MHz, due to the preparation of the population difference. Laser instability, of the order of 1-2MHz, will not move the centre frequency by more than ∼10% of the hole width on the time scales in these experiments. Hence with the laser at any frequency in the hole there will be an echo from the Raman Heterodyne rf experiment. This implies that with optical detection techniques the rf echo is not susceptible to the laser jitter, however the Raman technique is. In the Raman method the linewidth of the subgroup of ions affected by the optical pulses is $1/pulselength$ or in this case approximately 100kHz, 1% of the hole width. To have efficient echoes the light must continue to access this same subset of ions at each process period, that is during the pulses and read-out periods. However with the much narrower spectral linewidth of the optical coherence the experiment is sensitive to laser jitter. Any movement of the laser frequency means only a portion of the subgroup of ions is being affected by the optical pulses, not the full subgroup producing the echo. This leads to a false reading of the echo amplitude and an apparent faster coherence time.

4.3 Pseudo-Raman

The pseudo-Raman experiment also points to the difference in coherence time being due to the laser instability. The pulse sequence for this experiment is an equivalent rf $\pi/2$ pulse being applied optically and then after a delay an rf π pulse is applied. Any coherence generated by the optical pulse will then be rephased by the rf pulse. In this case though the coherence time is still shorter than the Raman Heterodyne, (1.3±0.1)ms compared to (4.2±0.8)ms. Since the lifetime of the optical transition is of the order of a few hundred

microseconds, after this time the system has forgotten that the coherence in the spin levels was created optically. This means the evolution of the spin levels in the pseudo-Raman experiment should be the same as in a normal Raman Heterodyne experiment. The only difference in the two systems is the spectral width of the excited group. In the case of the pseudo-Raman only a subgroup of ions are excited, with a linewidth of the order of a few hundred kilohertz. In the case of the Raman Heterodyne system though the linewidth of the system is approximately 10MHz. This larger linewidth is due to the fact that with the rf pulses, all the ions in the system are excited. The difference in the pseudo-Raman and the Raman Heterodyne results is then due to this difference in the spectral widths. The problem appears to happen in the time between the optical pulses and the read-out beam. Since the laser is quite unstable if there is a movement of the laser frequency between the time of the optical pulses and the read-out beam then this will mean that the echo amplitude being read-out isn't the amplitude of the entire subgroup that is being excited. The laser is perhaps only reading-out a side-wing of this subgroup. So the full coherence is lost which will mean that there is not a full echo being recorded.

Clearly with the Raman and pseudo-Raman methods laser jitter is an issue. At the moment we are not too concerned as to faster coherence time when echoes are created optically since this experiment will be repeated with a stable laser. It is possible for us to stabilise our laser down to $\sim$100Hz in 5ms and so is insignificant compared to the selected bandwidth of 100kHz. This should mean that the coherence times of the Raman echo then become longer than that of the Raman Heterodyne echo. The experiment should also be performed at the particular magnetic field that was discussed in previous chapters. At this field value the experiment will be much more sensitive and will enable us to see smaller interactions and differences between the two methods. Another way to make the experiment more sensitive is to have a better signal-to-noise ratio. This can be achieved in this experiment if the correct pulse sequence is used. As was shown in the theory chapter the best echoes are formed when the second pulse sequence is a 3-π pulse, rather than just 2-π pulses and this feature can be confirmed experimentally.

Conclusion

This project was aimed at investigating the effect operations on one group of ions would have on a different subgroup of ions in the crystal. In a quantum computer operations will be performed optically hence it was important to quantify the effect these optical operations would have on stored information. It was seen that there was no clear effect above uncertainties in the measurements. It was possible to experimentally determine an upper bound of 40Hz on the effect optical excitation of a subgroup of ions had on the coherence time of a separate group. This shift to the nuclear spin levels could possibly be caused by a number of effects. It was shown that the optical excitation of these ions would have caused a Stark shift of 2Hz to the nuclear spin levels. The largest change to the electric dipole moment due to the nuclear spin levels was determined to be 23mHzV^{-1}.

In order to perform gating operations it will be necessary to create coherence in the spin levels with optical techniques. This was proven to be possible with the achievement of Raman echoes. Raman echoes were obtained for the first time in the Laser Physics Centre and only the second time in a solid. Necessary improvements to the Raman technique were identified.

Appendix

6.1 N-V Centre

As stated previously, the initial project was focused on the N-V centre and the sources of decoherence in that lattice. Due to major equipment failures though, this system was abandoned in favour of the rare-earth Pr^{3+} ion.

6.2 Decoherence

The decoherence in this system can be caused by interactions in the crystal. The N-V centre has a nuclear magnetic spin and an electronic magnetic spin both equal to one. The associated electronic moment will be many times larger than the nuclear moment and consequently the centre will be much more sensitive to changes in the magnetic field in the surrounding environment than the case with Pr^{3+}. For this reason it is easy to couple the N-V centre to other centres.

In this case decoherence is due to spin-spin coupling; (i) nitrogen coupling to N-V centres, (ii) N-V/N-V coupling and also (iii) excitation of free electrons through optically exciting the nitrogen. Spin-spin coupling is where neighbouring similar spins undergo energy conserving spin 'flip-flops'. If this occurs there is a magnetic dipole-dipole interaction between the two spins and they exchange their spin states. This causes an alternating magnetic field at the N-V centre and so the energy of the system is changed, resulting in decoherence. (i) When we have nitrogen coupled to N-V centres the two coupled nitrogen ions in the lattice undergo this spin 'flip-flopping' so that the energy is conserved. The N-V centre will only 'see' one of the nitrogens spin-flip, since the other will be further away. Hence there will be a changing magnetic field at the N-V centre due to this magnetic dipole-dipole interaction. This changing magnetic field creates a slight change in the energy levels of the N-V due to the Zeeman effect. The changing energy levels means there is then a change in the frequency of the transition of interest, resulting in a modulation in the N-V frequency and causing decoherence. (ii) N-V coupling is the same principle as this, in this case there are two N-V centres that undergo the mutual spin-flip. This N-V coupling may lead to a shorter T_1, that is the lifetime of the population of the level will be shorter. It is the ensemble of spins that is the focus though. Subsequently there is no change in the overall population of the different spin states after a spin-flip and so there is a reduction in T_2, the coherence time, instead. This can be seen in the figure 6.1. (iii) The final effect on decoherence in the N-V system is the free electrons that are excited when the nitrogen ions are optically excited. Electrons are then able to move around in the conduction band of the lattice and so there will be a change to all the energy levels of

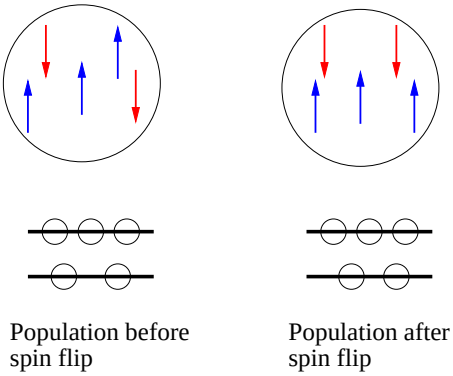

Figure 6.1: N-V Coupling

the N-V systems. This change will be the same to all the levels due to the Zeeman effect and so is a gross change that affects the frequencies of the transitions of interest.

The N-V centre has the unique peculiarity of spin polarising under white light. This means that all the spins states are optically pumped into the ground state spin level. Which has the effect of reducing any resonant spin-flipping processes between the N-V centres, which eliminates process (ii) above. It was expected that the application of a perturbing light field in this case would have a positive effect on the coherence time, unlike the Pr^{3+} system. Our preliminary investigations showed this was not the case though. With no perturbing light the coherence time of the system was measured as $(7.8\pm1)\mu$s, while the table 6.1 below shows the effect of different wavelengths of the perturbing beam on the system. A variety of different wavelengths of this second perturbing beam were

Wavelength (nm)	Coherence Time (μs)
600	7.4±0.9
623	5.6±0.9
518	2.9±0.8

Table 6.1: Coherence times with a perturbing light field

applied to the sample. A large perturbation occured with a 518nm second beam. This gave a coherence time of $(2.9\pm0.8)\mu$s compared to the unperturbed case of $(7.8\pm1)\mu$s. The bluer the light we shone on the sample, the greater the reduction to the coherence time. The below figure 6.2, [28], shows the absorption band of the type Ib diamond with the irradiated case on the left. This irradiation produces the N-V centres, while on the right the plot is of the unirradiated case with nitrogen impurities. The type Ib diamond on the left is representative of the diamond we use, where the concentration of our sample is $6.48\times10^{17}e^{-}/cm^{2}$. From this we see that the 600nm and 518nm wavelengths have similar absorptions at these two wavelengths. The plot on the right shows the absorption for a type Ib diamond, where substitutional nitrogen is the main impurity. Unfortunately in this plot the energy has been reversed. In this instance the absorption is the underlying nitrogen ions rather than the N-V centres, here we see that the 518nm wavelength will hit the absorption band as it starts to increase at approximately 2.5eV. The 600nm will have no real affect on the nitrogen as it will hit the band at approximately 2eV. From these two plots it is apparent that the bluer light will be ionising the nitrogen impurities in the crystal, while the higher wavelength light has no affect. A bigger reduction in the coherence time should be seen at even lower wavelengths, which would be a facet to

investigate.

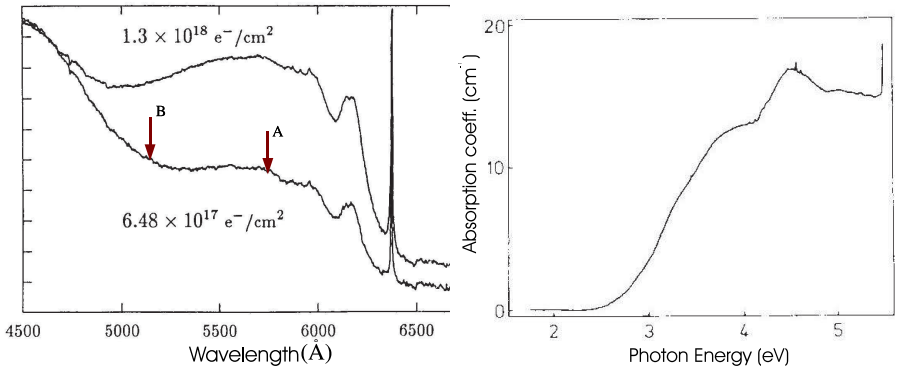

Figure 6.2: Absorption Band

Ionising the nitrogen impurities has the effect of creating a "semi-conductor" type material. The electrons are moving through the crystal in the conduction band, creating fluctuating magnetic and electric fields. It could also be possible for these electrons to move close to the N-V centres in the sample, meaning there is then a large electric dipole moment close to the N-V centre, contributing to the dephasing due to the magnetic field associated with the electron spin. Further experiments were hoped to be performed with pulsed light as opposed to cw, but due to the major equipment failures this had to be abandoned.

As can be seen there is a dramatic effect on the coherence time which has significant implications for the use of the N-V system in the quantum computing field. However I was unable to finish complete systematic measurements so am unable to be conclusive. This study will be taken up with a degree of urgency, in the Laser Physics Centre when the equipment becomes available.

Bibliography

[1] D.P. DiVincenzo. Quantum computation. *Science*, 270:255, 1995.

[2] K. Ichimura. A simple frequency-domain quantum computer with ions in a crystal coupled to a cavity mode. *Optics Communicaions*, 196:119, 2001.

[3] B.E. Kane. A silicon-based nuclear spin quantum computer. *Nature*, 393:133–137, 1998.

[4] G.J Milburn and B.E. Kane. Quantum computers. *Australian and New Zealand Physicist*, 35:191–196, 1998.

[5] M. Sellars. private communication, 2002.

[6] Ohlsson N., Mohan R.K., and Kröll S. Quantum computer hardware based on rare-earth-ion doped inorganic crystals. *Opt. commun.*, 201:71, 2002.

[7] A.A. Kaplyanskii and R.M Macfarlane, editors. *Spectroscopy of Solids Containing Rare Earth Ions: Coherent transient and holeburning spectroscopy in rare-earth ions*, volume 21. Elsevier Science Publishers, 1987.

[8] E. Fraval, M.J. Sellers, and J.J. Longdell. Demonstration of long hyperfine coherence times in $Pr^{3+} : Y_2SiO_5$. private communication, 2002.

[9] R.W. Equall, R.L. Cone, and R.M. Macfarlane. Homogeneous broadening and hyperfine structure of optical transitions in Pr^{3+}:Y_2SiO_5. *Phys. Rev. B*, 52:3963, 1995.

[10] A.J. Meixner, C.M. Jefferson, and R.M. Macfarlane. Meausrement of the Stark effect with subhomogeneous linewidth resolution in Eu^{3+}:$YAlO_3$ with the use of photon-echo modulation. *Phys. Rev. B*, 46:5912–5916, 1992.

[11] L.L. Wald, E.L. Hahn, and M. Lukac. Fluorine spin frozen core in Pr^{3+}:LaF_3 observed by cross-relaxation. *J. Opt. Soc.Am. B*, 9:789–793, 1992.

[12] M. Sellars and E. Fraval. private communication, 2002.

[13] J. Huang, J.M. Zhang, A. Lezama, and T.W. Mossberg. Excess Dephasing in Photon-Echo Experiments Arising from Excitation-Induced Electronic Level Shifts. *Phys. Rev. Lett.*, 63:78, 1989.

[14] S.B. Altner, M. Mitsunaga, G. Zumofen, and U.P. Wild. Dephasing-Rephasing Balancing in Photon Echoes by Excitation Induced Frequency Shifts. *Phys. Rev. Lett.*, 76:1747–1750, 1996.

[15] E.L. Hahn. Nuclear Induction Due to Free Larmor Precession. *Phys. Rev.*, 77:297, 1950.

[16] J. Mlynek, N.C. Wong, R.G. DeVoe, E.S. Kintzer, and R.G. Brewer. Raman Heterodyne Detection of Nuclear Magnetic Resonance. *Phys. Rev. Lett.*, 50:993–996, 1983.

[17] K.P. Leung, T.W. Mossberg, and S.R. Hartmann. Observation and density dependence of the raman echo in atomic thallium vapor. *Opt. Commun.*, 43:145–150, 1982.

[18] B.S. Ham, M.S. Shahriar, M.K. Kim, and P.R. Hemmer. Spin coherence excitation and rephasing with optically shelved atoms. *Phys. Rev. B*, 58:R11825–R11828, 1998.

[19] N.A. Kurnit, I.D. Abella, and S.R. Hartmann. Observation of a Photon Echo. *Phys. Rev. Lett.*, 13:567, 1964.

[20] C. Wei, S.A. Holmstrom, N.B. Manson, J.P.D. Martin, X.-F. He, P.T.H. Fisk, and K. Holliday. Raman Heterodyne Detected Magnetic Resonance: I. CW and Coherent Transient Measurements. *Appl. Magn. Reson.*, 11:521, 1996.

[21] J.J. Longdell, M.J. Sellars, and N.B. Manson. Hyperfine interaction in ground and excited states of praseodymium-doped yttrium orthosilicate. *Phys. Rev. B*, 66:035101, 2002.

[22] B.A. Maksimov, Y.A. Kharitonov, V.V. Ilyukhin, and N.V. Belov. Crystal Structure of the Y-Oxysilicate $Y_2(SiO_4)O$. *Soviet Physics-Doklady*, 13:1188–1190, 1969.

[23] J.A. Pople, W.G. Schneider, and H.J. Bernstein. *High-resolution Nuclear Magnetic Resonance*. McGraw-Hill Book Company, 1959.

[24] M.D. Levenson and S.S. Kano. *Introduction to Nonlinear Laser Spectroscopy*. Academic Press Inc., 1982.

[25] D.F. Walls and G.J. Milburn. *Quantum Optics*. Springer-Verlag, 1994.

[26] M. Sellars. *Ultra-High Resolution Laser Spectroscopy of Rare-Earth Doped Solids*. PhD thesis, ANU, 1995.

[27] A.V. Turukhin, V.S. Sudarshanam, M.S. Shahriar, J.A. Musser, B.S. Ham, and P.R. Hemmer. Observation of Ultraslow and Stored Light Pulses in a Solid. *Phys. Rev. Lett*, 88:023602, 2002.

[28] Collins A.T., editor. *The electronic and optical properties of diamond, Proceedings of the International School of Physics*, Amsterdam, 1997. IOS Press.